Flexural Modeling of the Colville Foreland Basin, Northern Alaska

Muhammad Hassan Quddusi[1] and Mortaza Pirouz[1]

[1]The University of Texas at Dallas

November 23, 2022

Abstract

In this study, we model the flexure of the Colville foreland basin in northern Alaska and calculate the effective elastic thickness (Te) of the Arctic Alaska terrane with a simple 3D flexural model. Previous studies show that the elastic thickness of northern Alaska is 65 km; however, the wavelength of the Colville foredeep is considerably shorter for such an elastic thickness and indicates a thinner elastic thickness for the area. Seismicity of crust, as a direct indicator of the mechanical strength, reduces considerably at a depth of 25 km in northern Alaska. We address these contrasting observations with a 3D flexural model to better understand elastic thickness constraints for the north of the Alaska lithosphere. We constrained Colville basin geometry with a structural map of the foredeep, where the maximum depth reaches 8 km towards the southwest of the basin. The flexural deflection model of northern Alaska considers various parameters, and results are compared to the observed data to obtain the best fit model. We applied basin and topographic loads, including a crustal root load with a ratio of 3.4-4.5 times to modern topography. Our obtained elastic thickness value is 13-16 km, with less than a 3% average misfit between the model and the observation. The results of this study indicate that the Colville basin geometry is mainly controlled by loads of the Brooks Range and basin deposits, and additional loads or density anomalies in the crust are not required for the deflection of the basin.

Flexural Modeling of the Colville Foreland Basin, Northern Alaska

M.H. Quddusi[1], and M. Pirouz[1]

[1]Department of Geosciences, The University of Texas at Dallas, Richardson, Texas, USA

Corresponding author: Muhammad Quddusi (hassan.quddusi@utdallas.edu)

Key Points:

- The elastic thickness of the Arctic Alaska microplate is 13-16 km
- No influence of subsurface dynamic loads on the bending plate
- A simple 3D flexure model predicts accurate deflection of the Colville foreland basin

Abstract

In this study, we model the flexure of the Colville foreland basin in northern Alaska and calculate the effective elastic thickness (Te) of the Arctic Alaska terrane with a simple 3D flexural model. Previous studies show that the elastic thickness of northern Alaska is 65 km; however, the wavelength of the Colville foredeep is considerably shorter for such an elastic thickness and indicates a thinner elastic thickness for the area. Seismicity of crust, as a direct indicator of the mechanical strength, reduces considerably at a depth of 25 km in northern Alaska. We address these contrasting observations with a 3D flexural model to better understand elastic thickness constraints for the north of the Alaska lithosphere. We constrained Colville basin geometry with a structural map of the foredeep, where the maximum depth reaches 8 km towards the southwest of the basin. The flexural deflection model of northern Alaska considers various parameters, and results are compared to the observed data to obtain the best fit model. We applied basin and topographic loads, including a crustal root load with a ratio of 3.4-4.5 times to modern topography. Our obtained elastic thickness value is 13-16 km, with less than a 3% average misfit between the model and the observation. The results of this study indicate that the Colville basin geometry is mainly controlled by loads of the Brooks Range and basin deposits, and additional loads or density anomalies in the crust are not required for the deflection of the basin.

Plain Language Summary

The Earth's outermost solid layer is called the lithosphere, which bends in response to the weight of the mountain on the Earth's surface and the gravitational pull of high-density mantle in the subsurface. The elastic strength of the plate defines the shape of the deflection. We calculate the wavelength of this bending and thickness of the lithosphere, which behaves as an elastic plate, and compared it with the observation. In this study, we used a 3D modeling code to calculate the elastic thickness of the lithosphere in northern Alaska, where the Arctic Alaska plate bends downward in response to the weight of the Brooks Range mountains and the Colville foreland basin. The results of this study indicate that the elastic thickness of the lithosphere in northern Alaska is 13-16 km. The low value of elastic thickness suggests that the north Alaska lithosphere has thin elastic strength.

1. Introduction

Foreland basins in collisional zones are associated with down warping of the lithosphere as a result of the loading of mountain front and accumulating sediments in the basin (Beaumont, 1981; DeCelles, 2012; Karner & Watts, 1983), and their architecture offer essential insights into the mechanical strength of the lithosphere. Subsurface loads may also contribute to loading, either by static (e.g., density variations of the subducting slab and the associated lithospheric root) or dynamic forces supported by mantle flow (Garcia-Castellanos, 2002; Pirouz et al., 2017). In this study, we focus on the Colville foreland basin underlying the east-west trending North Slope of Alaska (Figure 1). This basin is formed in response to the Brooks Range orogeny due to collision and clastic volume shed between the Arctic Alaska microplate and an oceanic island-arc in the Jurassic and Early Cretaceous (Box, 1985; Bird & Molenaar, 1992; Houseknecht, 2019; Moore et al., 1994).

Geometry and sedimentary record of the Colville basin play a significant role in exploring the dynamics of the northern Alaska and geomechanics of the lithosphere. Comparing the Colville basin’s wavelength with modern systems like Zagros and Taiwan enables us to have the first order of lithospheric elastic thickness estimation. The Zagros foreland basin width is approximately 450 km and elastic thickness about 50 km (Pirouz et al., 2017), and in the Taiwan foreland basin, the basin width is 110 km; and elastic thickness is 13 km (Lin & Watts, 2002). The elastic thickness for the Colville basin with 200 km width is identified as 65 km (Nunn et al., 1987); however, by comparison with other foreland basins, it seems reported elastic thickness for this basin is considerably overestimated concerning the basin wavelength.

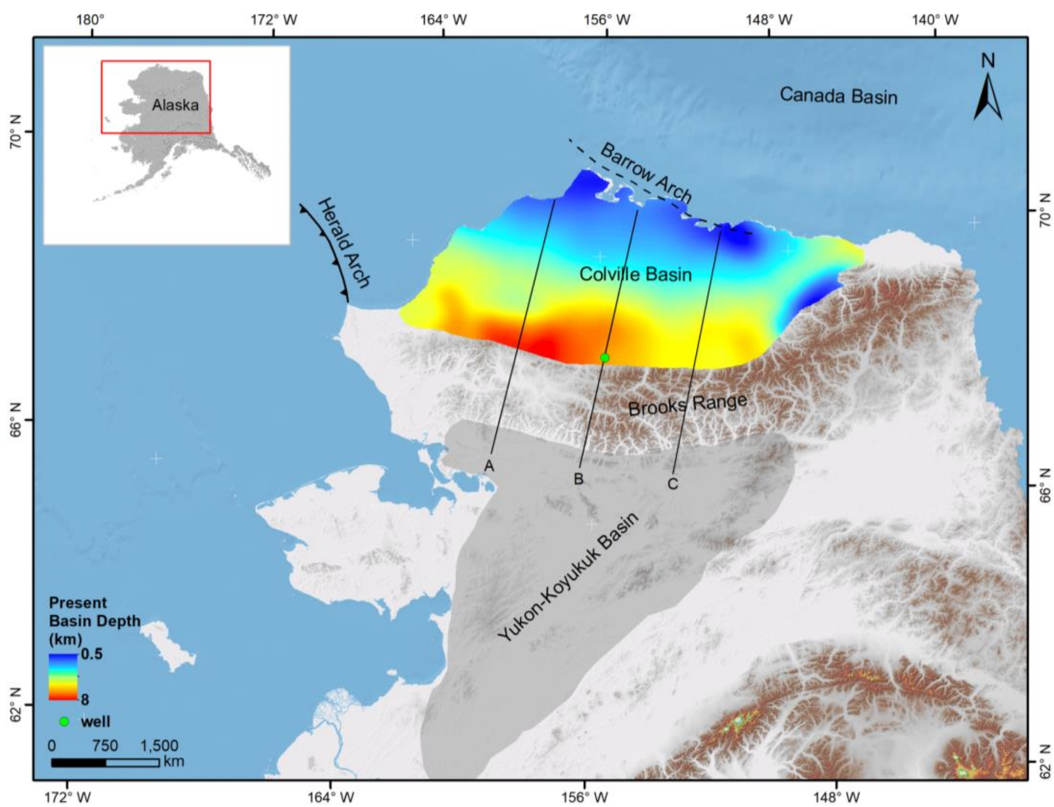

Figure 1. Modern plate setting of northern Alaska. Brooks Range fold and thrust belt are flanked on the north and south by Colville and Yukon-Koyukuk foreland basins. The observed Colville foreland basin depth is adopted from (Bird & Houseknecht, 2011).

A recent study involves 3D forward modeling of crustal density variations and Bouguer anomalies of whole Alaska carried out by Torne et al. (2020). Their results highlight thick crust about 45 km beneath the Brooks Range, and beneath the Colville basin, it gradually decreases by a few kilometers. Furthermore, seismic events that mostly take place in the brittle zone of the crust (Maggi et al., 2000) can also be used to rough constrain the elastic strength of the lithosphere. In the Arctic Alaska region, the frequency of earthquakes drops dramatically at a depth of 25 km; this observation is difficult to reconcile with the proposed 65 km elastic thickness by Nunn et al. (1987).

The first deflection study in the Alaska region was carried out by Nunn et al. (1987) by modeling a simple 2-D flexure of the Colville foreland basin. Their results suggest that the topographic and basin loads are insufficient to produce the observed deflection, and gravity signals are characterized by a local gravity minima representing mass deficit beneath the belt and basin. They inferred that an additional subsurface load is required to make present-day basin geometry. In this study, we estimate the effective elastic thickness (Te) of the northern Alaska lithosphere and address how the geometry of the Colville foreland basin relates to the orogenic loads posed by the Brooks Range fold and thrust belt. We constrain the 3D geometry of the Colville foreland basin with a published structural map of the foreland depth (Bird & Houseknecht, 2011). We model the flexure of northern Alaska using a simple 3D elastic plate flexural bending model. Besides, we also evaluate the possibility of additional subsurface loads. To validate the computed elastic thickness from the flexural model, we calculate free-air gravity anomalies from the obtained flexural model and compare it to the observed gravity data. We show that a flexural model based on the weight of the Brooks Range and the Colville foreland basin fits well with the observed present-day geometry of the foreland and the gravity data. Recent studies show that 3D flexural solutions constrain better results for basin geometry, spatial/temporal variations in crustal parameters, and elastic thickness compared with 2D models by applying a more realistic load of topography and basin deposits (Curry et al., 2019; Pirouz et al., 2017). A recent reconstruction of the Arabian plate deflection using a 3D approach shows that the topographic and basin loads and the weight of crustal root models an accurate foreland basin geometry (Pirouz et al., 2017). Geological observations in forward flexural modeling reconstruct better estimates for lithospheric elastic thickness to compare with gravity data. In contrast, observed gravity offers better insights for calculating the load posed by the crustal root (Pirouz et al., 2017).

2. Geological and Geophysical Framework

2.1. Tectonic Evolution

Alaska is a landmass formed by an amalgamation of several litho-tectonic terranes of varying origins that were thoroughly assembled by the Late Cretaceous (Fuis et al., 2008; Moore & Box, 2016; Plafker & Berg, 1994). During the Jurassic and Early-Cretaceous, two major tectonic events dominated northern Alaska. In the Early-Cretaceous, the Arctic Alaska microplate collided with an oceanic arc-continent complex and bent downward in response to the collision. Simultaneously, on the opposite side of the plate, towards the east, rifting occurred that led to the opening of the present-day Canada basin (Mayfield et al., 1983; Sweeney, 1985). By the Mid-Cretaceous, the collision resulted in the Brooks Range fold and thrust mountain belt and the associated foredeeps on both sides of the range (Figure 1). The evolution of Arctic Alaska was accompanied subsequently by counterclockwise rotation due to the opening of the Canada Basin. Although the counterclockwise rotation model of Arctic Alaska and nearby terranes have been a topic of debate, nonetheless, it is the most widely accepted and plausible explanation of the present-day tectonic setting. For example, using geological and geophysical data Embry (1990) also supported the hypothesis of the counterclockwise rotation model. An extensive discussion of all the terrane nomenclature of Alaska is beyond the scope of this study; the reference is made to (Fuis et al., 1997; Fuis et al., 2008; Moore et al., 1994; Moore & Box, 2016; Plafker & Berg, 1994) where a compilation of most of the existing literature on the subject can be found.

The Present-day North Slope of Alaska consists of the Arctic Alaska terrane that constitutes the Brooks Range fold and thrust belt and the Colville foreland basin (Figure 1) north of the Brooks Range (Bird, 2001; Moore et al., 1994; Miller, 1994; Plafker & Berg, 1994). Towards the south of the Brooks Range lies a Cretaceous age foreland basin called the Yukon-Koyukuk basin that extends into the western Alaska region (Patton & Box, 1989). This range is about 1000 km long and 300 km wide arcuate belt consisting of a series of imbricate thrust sheets with obduction of ophiolites emplaced onto the southward (present coordinates) subducting continental Arctic Alaska terrane. The estimated 580 km of crustal shortening occurred in some parts of the Brooks Range (Mull, 1982; Nunn et al., 1987; Patton et al., 1994). The northern boundary of the Colville basin is an Atlantic-type rifted continental margin (Grantz et al., 1994; Grantz & May, 1982) that extends into the shoreline of Alaska where a broad subsurface basement ridge, the Barrow Arch, developed during the rifting episode from Jurassic to Early Cretaceous. The basin extends offshore toward west under the Chukchi Sea into the northwestward-trending Herald Arch and the northward-trending Chukchi platform. These geological features are remnants of a late Paleozoic to Early Mesozoic south-facing Arctic continental margin. On the far east, the basin narrows down along the Alaska-Canada border (Bird, 2001).

2.2. Tectonostratigraphic Sequences

The North Slope of Alaska is underlain with rocks as early as the Late Proterozoic. Stratigraphic records of the North Slope of Alaska is subdivided into four primary sequences based on tectonic history, genetic relations, and origin (Bird, 2001; Hubbard et al., 1987). The oldest sequence, the Franklinian sequence, holds a clue to complex geologic history due to deformation caused by Ellesmerian orogeny. This sequence mostly consists of a Pre-Devonian deformed and metamorphosed basement complex (Bird & Houseknecht, 2011; Grantz & May, 1982). The basement complex is shallower near the Barrow Arch and is most profound at the northern edge of Brooks Range. A regional unconformity developed with the Ellesmerian orogeny and the Ellesmerian sequence was deposited on the passive margin of the Arctic shelf. This sequence, from Mississippian to Triassic age, consists of carbonate and clastic continental shelf deposits (Bird, 2001). Syn-rift deposits characterized by stacked sequences of southward prograding clinoforms forms Beaufortian Sequence of Jurassic and Early Cretaceous. A prominent feature in this sequence is the break-up unconformity, also known as the Lower Cretaceous Unconformity (LC U), at the crest of the Beaufortian sequence. On a regional scale, this unconformity truncates the reservoir and seal rocks near the Barrow Arch, playing a vital role in hydrocarbon entrapments. More importantly, LCU defines the base of the oncoming clastic sediments of the Colville basin (Figure 2), which is essential for constraining the geometry of the Colville basin for flexural studies. Beaufortian is the last sequence which has the northerly source of sediments. The Brookian sequence is derived from the south due to the collisional orogeny of the Brooks Range. It comprises progradation cycles characterizing dramatic sea level rises and substantial shifts of paleo shoreline (Bird, 2001; Decker, 2007). Thick clastic sediments above 7620m (25,000 ft) are deposited into the Colville basin (Houseknecht et al., 2009).

2.3. Geometry of Colville Foreland Basin

Colville basin is about 200 km wide with maximum depths of 8 km adjacent to the Brooks Range toward its southern edge. A complete stratigraphic column of the Colville basin is shown in (Figure 2). The basin extends laterally from west to east spanning about 650 km area. The structural style of the basin is a tapered wedge that shallows up-dip towards its northern edge close to Barrow Arch, where the depth of the basin drops to 500 m. Investigation of seismic data shows massive prograding clinoforms sequences in the Nanushuk and Torok formations, indicating a high rate of sediment influx and large accommodation space in the Colville basin.

The seismic interpretation of the frontal Brooks Range and North Slope of Alaska shows evidence of significant detachment surfaces that developed during the Tertiary deformation phase affecting the southernmost part of the foredeep (Mull, 1982). The Kingak formation, which lies below LCU (Figure 2), separates foreland sediments from the passive shelf margin acting as a surface for thrust fault propagation and structural relief (Moore et al., 1994; Stier et al., 2014). Northward tectonic transport of Early Brookian fold and thrust belt is evident in the southern part of the Colville basin, which ceased possibly by Aptian (Moore & Box, 2016; Mull, 1982).

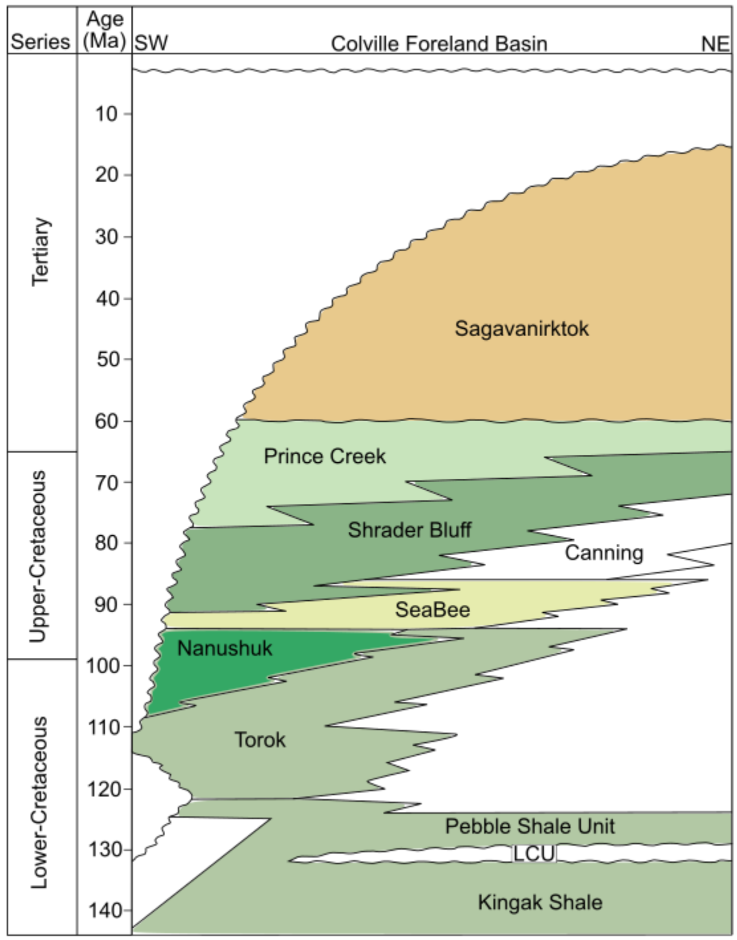

Figure 2. Stratigraphic column of the Colville basin. The Lower Cretaceous Unconformity LCU (ca. 133 Ma) is the regional unconformity separating Colville basin deposits from the passive margin. The Kingak shale constitutes the uppermost formation of the passive shelf margin.

2.4. Crustal Structure of Northern Alaska

Crustal architecture of continents is often studied using seismic tomographic imaging with active source experiments, e.g., S and P seismic receiver functions. In general, the Alaska continent shows substantial variability of crustal thickness due to variations in topography, multiple episodes of terrane accretion, and the influence of orogenic activity. Southern Alaska shows high variability of crustal thickness and more than 55 km crustal thickness observed near the Pacific margin, whereas central Alaska has an average of 32 km crustal thickness (Fuis et al., 2008). South and south-central Alaska is extensively imaged by seismic broadband due to the active subduction of the Pacific plate under Alaska (Miller et al., 2018). In contrast, the region north of the Brooks Range has been sparsely imaged mainly due to quiescence in recent tectonic activity.

(TACT) was the first experimental imaging of the Brooks Range (Trans-Alaska-Crustal-Transect: TACT) using seismic reflection and refraction methods covers an extensive profile from the south to north (1350 km) covering entire Alaska (Fuis et al., 2008). In the northern Alaska segment of TACT, the profile spanned from the coastal plains of Alaska through the Brooks Range. This study identified an asymmetrical crustal root beneath the Brooks Range with 46 km thick crust. The crustal evolution of northern Alaska is also defined by 3D modeling of Bouguer anomalies carried out by Torne et al. (2020), highlighting regional lows ranging from -140 to -60 mGal in the mountainous regions of the Brooks Range. This low regional trend extends north towards the Colville foreland basin, where Bouguer anomalies range from -60 to -20 mGal. The overall trend of regional low gravity anomalies highlights crustal thickening beneath the Brooks Range. Towards the north of the Colville basin, the gravity anomalies abruptly change from low to high values. The observed Bouguer anomalies near the shelf reach 180 mGal. This increase is attributed to the thinner crust of the Beaufort shelf that is formed due to the rifting of the Canada Basin.

3. Methods and Data

3.1. Flexure Model Description

The lithospheric flexure studies have been mainly developed on two principle methods; the forward modeling techniques (Cattin et al., 2001; Karner & Watts, 1983; Lyon-Caen & Molnar, 1983) and the inverse or spectral methods (Bechtel et al., 1990; Forsyth, 1985; Kaban et al., 2018;

Kirby & Swain, 2009; McKenzie & Fairhead, 1997). Recent advancements in computation have also enabled various improvements in the spatial and spectral methods. For example, the finite-element method (Arnaiz-Rodríguez et al., 2020; Simpson, 2017), the finite difference method (Garcia-Castellanos et al., 1997; Tesauro et al., 2012), and the analytical solutions based on the convolutional technique (Braitenberg et al., 2002; Wienecke et al., 2007). To calculate flexure underneath the Arctic Alaska plate, we assume an elastic plate inviscid over a dense asthenosphere in isostatic equilibrium (e.g., Turcotte & Schubert, 2002). The plate is flexed downward in response to the topographic load, with contributions from the adjacent sediment-filled foreland basin and the crustal root (Figure 3). An additional force also accompanies the downward flexure, called the hydrostatic restoring pressure, caused by the replacement of mantle rocks by lighter density crustal rocks. The crust beneath the load is effectively thickened by the amount by which the Moho is depressed.

For deflection calculation, we use a new approach introduced by Pirouz et al. (2017). They applied topographic load and basin load with density variation versus depth, and assume deflected lithosphere filled with air (Pirouz et al., 2017, 2020), and a load of crustal root applied individually with proportional ratio to topography (See figure 3; and see section 5.1 & 5.2 in Pirouz et al., 2017). This method reconstructs a better deflection pattern that fits the observation since it has been tested for several examples (Pirouz et al., 2020).

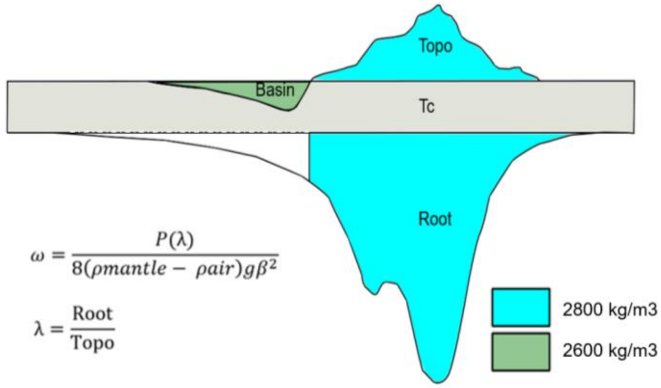

Figure 3. The conceptual model shows that the applied load is calculated from the excess thickness of the crust (topography and crustal root) and basin load colored in green. The equation calculates flexural parameters where Tc: the thickness of un-deformed crust, ω: max deflection, P: topographic load, $\rho mantle$: density of mantle, ρair: density of air, g: gravity acceleration, β: flexural parameter and λ is the ratio between the thickness of crustal root and topographic height (adopted from Pirouz et al., 2017).

The modeling approach used in this study is based on an analytical solution derived from computing the partial derivatives of the 4th order of the equations that describe the bending of an elastic plate. This method has been tested previously in the convergent zones (Wienecke et al., 2007; Pirouz et al., 2017), and the results are also consistent and comparable with conventional spectral methods. The main advantage convolutional technique bears against the spectral approach is that the result is stable in irregular topography with a high spatial resolution (e.g., Wienecke et al., 2007). See supplementary material for details (Text S1).

3.2. Flexure Data, Gravimetric Analysis, and Workflow

The first step to model the flexure is to constrain the present-day geometry of the Colville foreland basin, whose base is highlighted by a regional unconformity known as the Lower Cretaceous

Unconformity (LC U). In this study, we use a published structural map of LCU adopted from (Bird & Houseknecht, 2011) to constrain the present-day basin geometry (Figure 4a). A complete surface load on the bending plate is characterized by both sediment infill and the adjacent range topography. To estimate the current topographic load, we use high resolution 60×60 m raster elevation grid; DEM (Digital Elevation Model) derived from (EDNA - Elevation Derivatives for National Applications) by US Geological Survey (2005); and for the basin load, we used the foreland depth map to obtain sediment thickness and took into account the density variation of the basin load with depth to calculated applied force from the basin. The deflection at each point is calculated iteratively using the equations described in supplementary material, and the elastic parameters used in the calculations are summarized in Table 1. The flexure model is tested by changing the elastic properties of the plate, and three cases of density variations are tried, and the output is summarized in Table 2 in section 4.2.

A range of models has been calculated by stepwise increasing the elastic thickness values between 1 to 50 km. Similarly, the tested λ (root/topo ratio) ranges from 1 to 10, with a stepwise increase of 0.1. The iterative modeling approach is adopted to find the best fit between the observed and the predicted foreland depths by testing all possible solutions. The corresponding elastic thickness value at which the root-mean-square (RMSE) was minimum is the best fitting model. The deflection model is the predicted foreland surface derived from the flexure calculations.

Table 1. Summary of elastic paraments used in the calculation of the flexural model.

Constant	**Symbol**	**Value**	**Units**
Young's Modulus	E	1×10^{11}	Pa
Poisson's Ratio	σ	0.25	unitless quantity

Gravity Acceleration	g	9.81	m/sec^2
Mantle Density	$\rho mantle$	3300	kg/m^3
Crustal Density	$\rho crust$	2800	kg/m^3
Basin Density	$\rho basin$	2600	kg/m^3
Air Density	ρ_{air}	1.200	kg/m^3

3.3. Gravimetric Analysis and Workflow

Gravimetric measurements at the Earth's surface are significant for studies of lithospheric flexure. Gravity anomalies arising due to density variations in the lithosphere can be used to study the isostatic balance of mountains on the Earth's surface. There are two methods typically used to estimate the elastic thickness of the lithosphere with the gravity data (Watts, 2001). In forward modeling technique, known load structures, e.g., a sedimentary basin or a seamount, are used in a trial and error analysis to estimates the best fit elastic thickness of the lithosphere. In contrast, the inverse spectral method uses the relationship between the observed gravity and topography. The observed measures are subsequently inverted against the elastic plate predictions, giving estimates of elastic thickness and other lithospheric parameters (Eshagh et al., 2020; Forsyth, 1985). The estimates of elastic thickness from spectral methods are often over or under-estimated (McKenzie, 2010).

In this study, we also investigate the gravity signal of the Arctic Alaska microplate to validate our flexural model results. However, we do not employ the conventional spectral methods to estimate the effective elastic thickness; instead, free-air anomalies (FAA) are calculated from the flexure model itself and then compared to the observed anomalies. We utilize the FAA dataset available from World Gravity Map - WGM2012 (Bonvalot et al., 2012). WGM constitutes a set of gravity anomaly maps and digital grids computed globally from available reference Earth's gravity and the elevation models. The surface free-air anomaly dataset is derived from the EGM2008 Geopotential model and the ETOPO1 Global Relief Model. This dataset is a comprehensive free-air anomaly that considers most surface masses, including atmosphere, land, ocean, inland seas, lakes, ice caps, and ice shelves, and computations are based on accurate geodetic and geophysical definitions of gravity anomalies. The anomaly grid is computed with a $1' \times 1'$ resolution, and the reference density used for the Bouguer and the isostatic anomaly is 2670 km/m^3. Furthermore, we constrain the FAA using the Moho discontinuity boundary from the seismological Moho data of entire Alaska assembled by Torne et al. (2020) and compare to the observed FAA and calculated FAA form the best fitting deflection model. Calculations of the FAA are explained in the supplementary material (Text S2).

4. Results and Discussion

4.1. Flexure Model of Colville Basin

We present a simple 3D flexural model that reconstructs the Colville foreland basin geometry (Figure 4). To avoid discrepancies in the output results, we systematically modified and clipped regions of uplift and post-collisional deformation; for example, see two large antiforms (Figure 4a) that are ignored to compare the observed and the modeled foreland basin. A basement high, Barrow Arch, significantly affects the northern part of the Colville basin. As a result, structural relief of the foreland base abruptly changes between the high and low values. We exclude them to avoid possibly overestimated or underestimated the importance of the elastic thickness. Our model covers approximately 83,000 km^2 area of the basin exhibits an overall excellent correlation between the observed and modeled foreland geometry with some systematic misfit. The observed misfit is shown along three cross-sections A, B, and C in Figure 5. For detailed cross sections in the Colville foredeep and misfit map, see supplementary material (Figure S3 and S6).

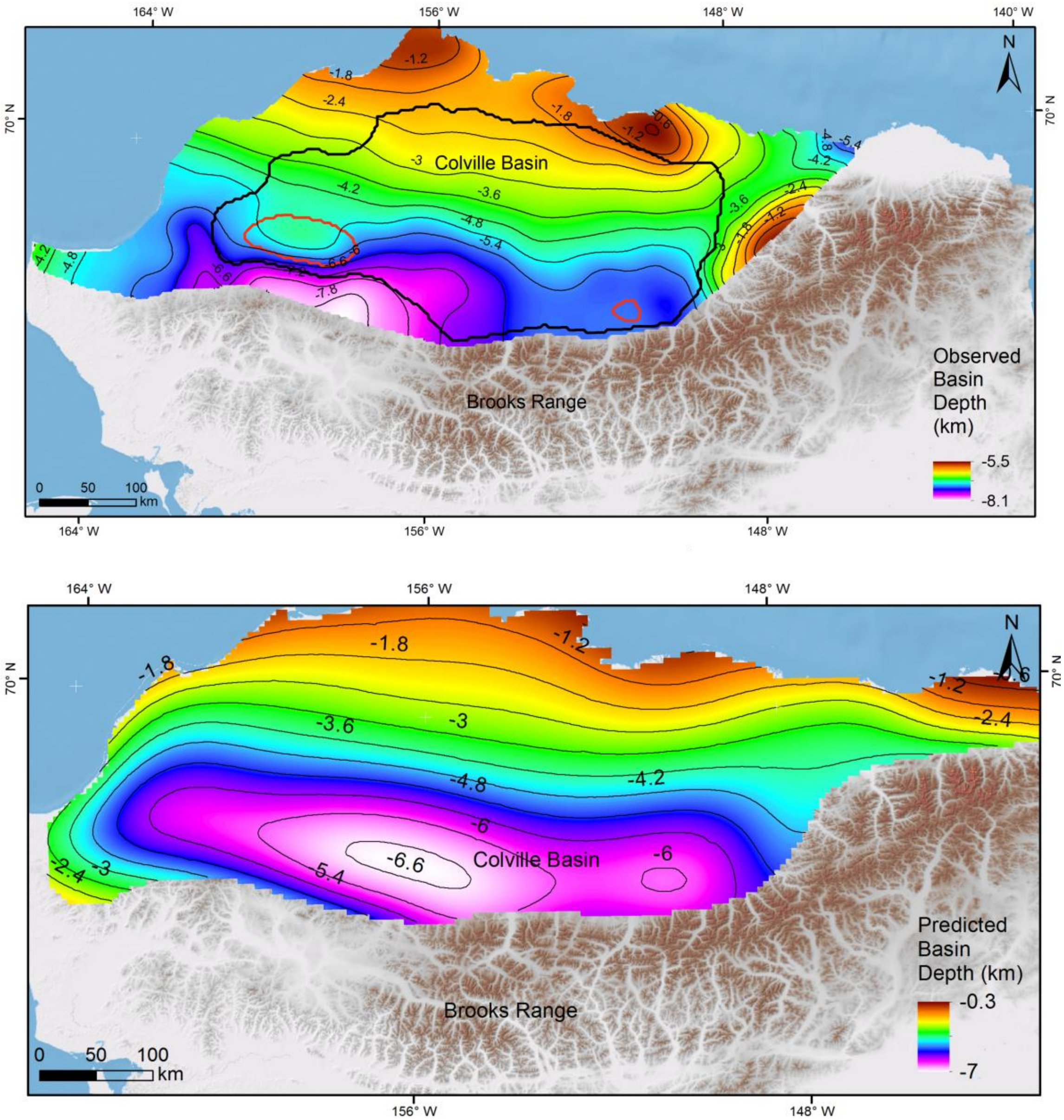

Figure 4. Observed (a) and best model predicted depth (b) of the base of foreland sediments of the Colville basin. The area excluded for RMSE calculation is shown in panel (a). Black polygon in panel (a) corresponds to the RMSE area and red polygons show excluded areas form the RMSE calculation.

Post-collisional deformation associated with the thrust front of the Brooks Range had minimal effect on the basin geometry. In this section, we emphasize the causes of misfits between the observed and modeled foreland depth and its important implications for the flexure model of the Colville foreland basin. Following the collisional orogeny, the Brooks Range thrust system experienced two significant phases of deformation. Early and Late Cretaceous tectonism is characterized by crustal shortening and low relief duplex structures (Houseknecht & Wartes, 2013; Moore et al., 2004; Wallace et al., 1997). The thrust belt also experienced a younger deformation phase in Early Tertiary time (Stier et al., 2014). During the second phase, the fold and thrust sheets were dominated by thick-skinned deformation. They consisted primarily of upright detachment folds, whereas towards the north of the range front, the Early Cretaceous strata of the Colville foreland basin experienced thin-skinned fold style deformation involving the formation of anticlines. (See figure 15 in Moore & Box, 2016). Note that we exclude this deformed part from RMSE calculation (figure 4a). The western part of the basin shows a weak correlation between the observed and predicted foreland depth. This discrepancy arises mainly due to the second phase of deformation, see Section A in figure 5a. Our model predicts shallower depths as compared to the observed foreland depth. Section B shows the slightest misfit in the modeled foreland depth near the northern part of the basin. We interpret this inconsistency as due to the uplifting effects of the Barrow Arch basement high (Figure 5b). The model result yields the best correlation with the observed data is shown in section C (Figure 5c), where the geometry of the foreland basin is relatively uniform. See more correlating sections in the supplementary material (Figure S2).

We carefully considered all the misfits in the flexural model and conclude that these inconsistencies are caused mainly by deformation processes and do not affect the robustness of the model results. Our flexural model implies that the surface load posed by the Brooks Range topography, a proportional subsurface crustal root associated with the orogen, and the overburden of the Colville basin sediments produce enough force to bend the Arctic Alaska microplate. We find that this model is very well correlated to the present-day foreland geometry of the Colville basin.

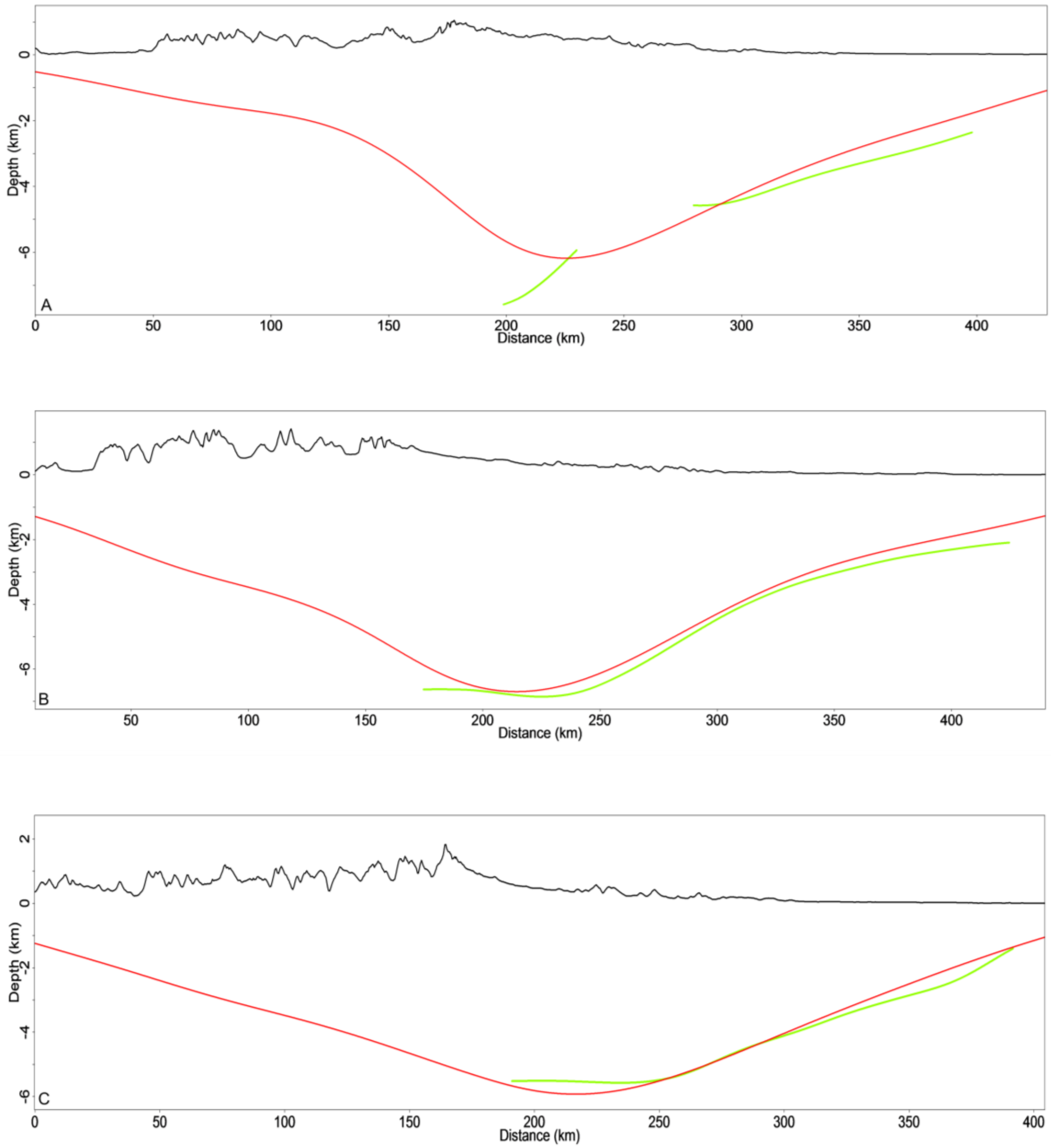

Figure 5. Cross-sections (A, B, and C) in the study area showing observed and predicted flexure of the Colville basin. The green line represents the observed depth to the LCU, and the red line represents the modeled depth to the LCU. See figure 1 for the location of sections.

4.2. Estimating Te value

The flexural model results provide a first-order calculation of the effective elastic thickness (Te) beneath the Colville foreland basin and offer insights into the long-term elastic strength of the Arctic Alaska lithosphere. The optimum value of Te is modeled by considering various elastic parameters (Table 1). A significant varying elastic parameter is a function of density contrast between the crust and mantle $\Delta\rho$. To obtain reliable density variation and unformed crustal thickness, we obtained the FAA from the observed Moho depth (Torne et al., 2020) for a different range of values for the mentioned variables. Our results show that $\Delta\rho = 300$ kg/m^3 works best where the minimum crust thickness is about 35 km (Miller et al., 2018). See supplementary material figure S1. Our models indicate that the misfit error (RMSE) between the observed and predicted foreland depth is lowest when ($\Delta\rho$) is minimum, and the corresponding Te value is 13 km (Table 2). Solutions that still correlates precisely with the basin geometry (less than 3% error) results from $\Delta\rho$=300-500 kg/m^3, where the mantle density is about 3200-3300 kg/m^3, and the average crustal density is 2800 kg/m^3 (Torne et al., 2020). We tuned the best fit models with constant and varying elastic parameters (Table 1 and 2). Our models specify that the Arctic Alaska microplate deflection can be realistically defined with a subsurface crustal root that is 3.4 - 4.5 times the modern topography of the Brooks Range mountain. Misfit error between the observed and modeled foreland geometry is less than 3 %, and the best fit Te value of 13-16 km (Figure 6). FAA data is also used to model elastic thickness, but it does not precisely emphasize the elastic thickness value like the geologic observation. In figure 7, we show the comparison between the modeled FAA and the observed FAA. Note that changing 1.5 mGal in root mean square error value will result in elastic thickness values between 40 and 100 km. However, it defines a better ratio between topography and crustal root, which is about 4.5 for different elastic thickness values.

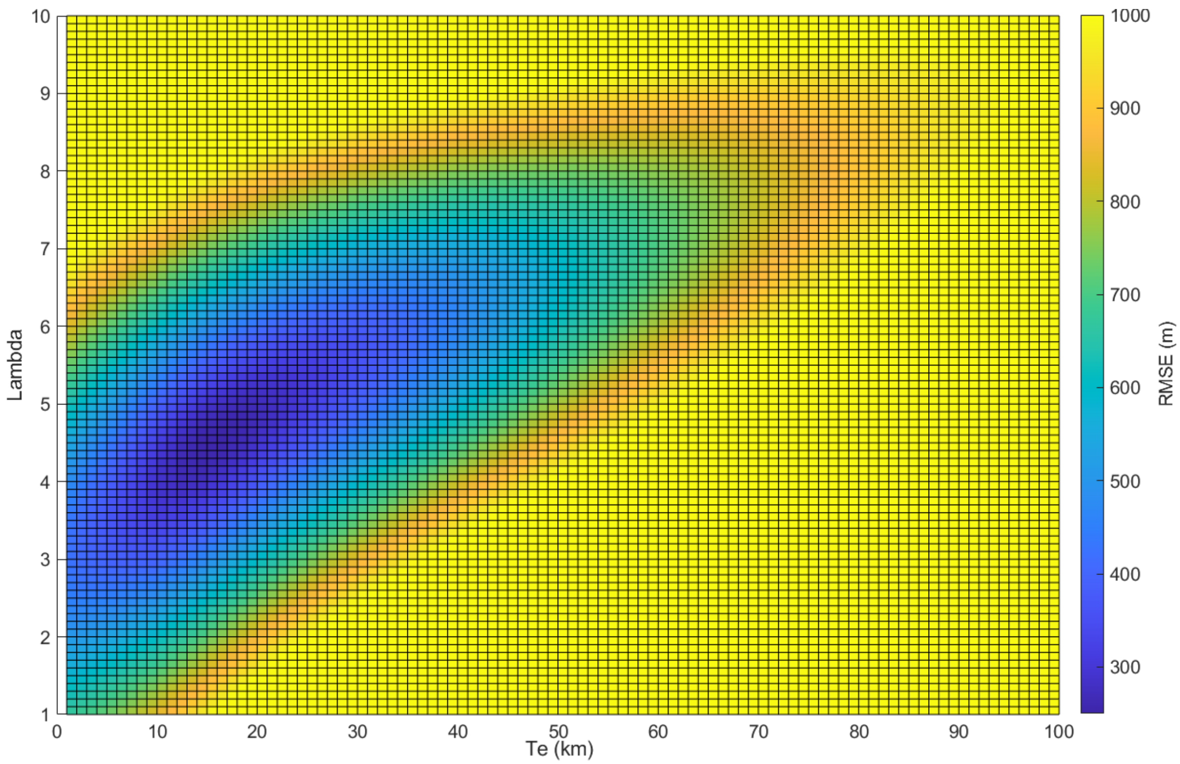

Figure 6. Root Mean Square Error (RMSE) between modeled and observed foreland depths as a function of an elastic thickness (Te) and dimensionless scaling factor between root and topography (λ)

Table 2. Summary of modeling results using different density variation between mantle and crust. Obtained root to topography ratio, elastic thickness, RMSE of deflection models is listed below for five models.

Density Variation $\Delta\rho$ (kg/m^3)	Root/Topo Ratio (λ)	Te (km)	Deflection RMSE (m)
700	5.8	21	327
600	5	16	285
500	4.5	16	252
400	3.9	14	225
300	3.4	13	205

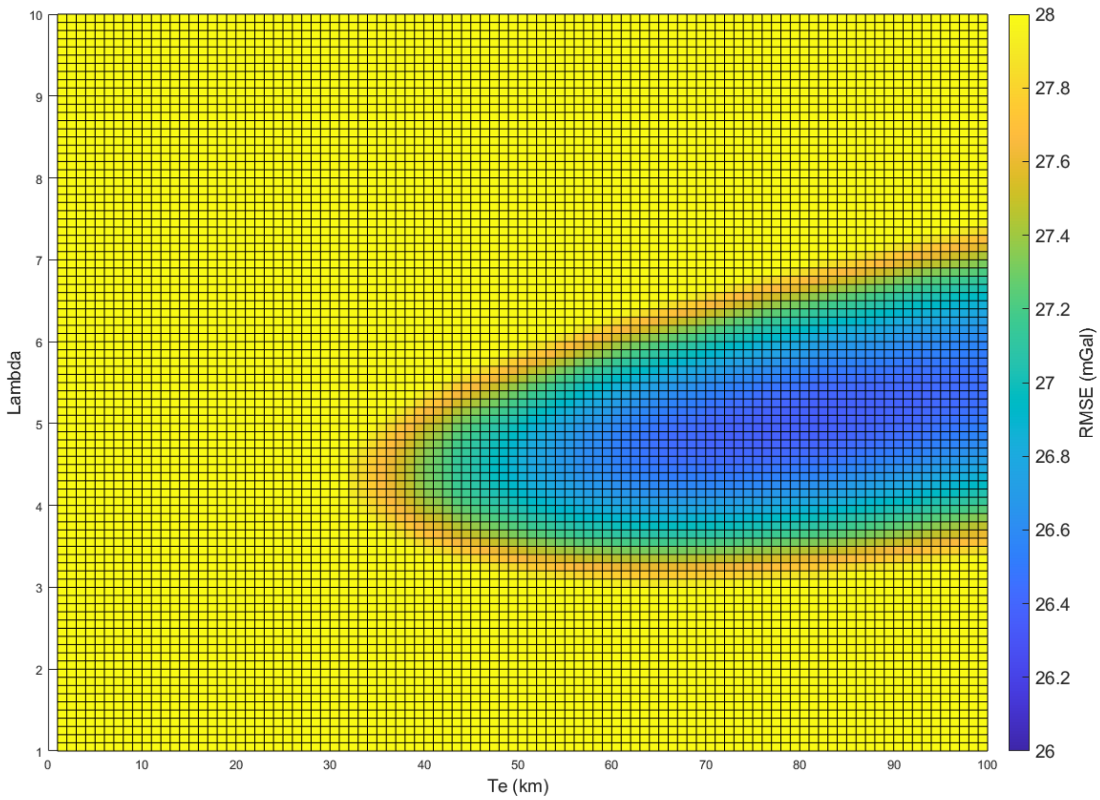

Figure 7. Root Mean Square Error (RMSE) between observed and modeled FAAs. Note the small change, 2mGal, in RMSE between observed FAA and models highlights a wide range of elastic thickness, e.g., Te=40 to 100 km, and relatively better construction for crustal root -topography ratio.

Elastic thickness is a first-order proxy for the lithospheric strength, and low lithospheric strength results in a narrow and deep foreland basin (Burov & Diament, 1995; Watts & Burov, 2003). The Arctic Alaska lithosphere poses low resistance to the surface and subsurface-induced loads resulting in a deep short-wavelength basin. Our result shows that 13-16 km of elastic thickness for the Arctic Alaska lithosphere produces a basin that matches the observation. Our average misfit between model and observation is less than 252 meters in a basin with more than 6 km depth (about 3%).

The computed Te value for northern Alaska is low compared to other foreland basins such as Appalachians and Zagros. However, it is within the range of many reported Te values of foreland basins (Curry et al., 2019; Fosdick et al., 2014; Haddad & Watts, 1999; Lin & Watts, 2002). Simple observation and comparison between the Colville basin's wavelength with active collisional zones like Zagros also support the flexural model's results. The wavelength of the Zagros foreland basin is approximately 450 km, and the reported elastic thickness is about 50 km (Pirouz et al., 2017). In the Taiwan foreland basin, these values are 110 km and 10-13 km, respectively (e.g., Lin & Watts, 2002). Considering these observations, computed 13-16 km Te with 200 km wavelength of the Colville basin fits this simple analysis well.

In general, old foreland basins have a large elastic thickness, but having a weak lithosphere in the old basin is also possible. Foreland basins may inherit the low elastic thickness values as they migrate over a passive margin and remain low for extended durations (Watts, 1992; Watts & Burov, 2003; Angrand et al., 2018). In northern Alaska, we believe that during the collision of Arctic Alaska terrane with the oceanic arc in Jurassic, the bending Arctic Alaska microplate inherited the low elastic thickness and has considerably remained low after collisional tectonics ended. Collision on the southern side of the plate (pre-rotation coordinates) started at the same time as the arctic Alaska plate rifted away from the passive margin on its northern edge (Mayfield et al., 1983; Sweeney, 1985), as shown by Desegaulx et al. (1991), we also believe it is likely that the lithosphere and the foreland basin in northern Alaska acquired the size and width due to the thermal state of ongoing rifting.

The rheological models affecting the long-term strength of an elastic lithosphere has long been a topic of debate. The most widely accepted rheological models are; Crème Brulee (Jackson, 2002), where the strength of the lithosphere mainly resides in the upper crust and mantle is considered weak for accommodating long term stresses. On the other hand, the Jelly sandwich model (Afonso & Ranalli, 2004; Burov, 2006) more realistically explains the multi-layer rheology of the Earth's lithosphere. An important implication of these models is that the crust is either coupled or decoupled from the upper mantle. The elastic thickness of a plate, as a result, is dependent on the mechanical behavior of crust and mantle. A strong coupling between the crust and mantle suggest high Te values; on the other hand, low Te values are associated with a mechanically decoupled lithosphere (Brown & Phillips, 2000). We believe that strong driving forces in the mantle are necessary for Alaska because the continent has a complex tectonic history of orogenesis and accretion of far traveled terranes. In northern Alaska, this view agrees with the presence of a thick lithosphere beneath the Brooks Range, as shown by Torne et al. (2020). Our results, therefore, support strong upper mantle rheology, which in the case of northern Alaska, is decoupled from the lower crust. However, our results do not support the idea of high elastic strength and a strong cold lithosphere, as postulated by Torne et al. (2020). Contrarily, the flexural model results show weakness in the elastic strength. Low Te suggests that the mechanical weakness is possibly due to the lithospheric extension associated with the rifting on the opposite side of the Arctic Alaska microplate that initiated the collision forming the Brooks Range and the Colville basin.

4.3. Implication for Subsurface Load

Accounting for sediment density variations as one of the subsurface load sources is critical for calculating the right amount of applied force on the lithosphere, especially in low topographic regions (e.g., see Kaban et al. 2018; Kirby & Swain, 2011; Pirouz et al., 2017). Thick Colville sedimentary cover has a significant effect on the deflection, which we incorporated this vertical variation into the flexural model using the borehole data; for details, see supplementary material (Figure S1). Based on our flexure model, the static load associated with the Brooks Range, sediment infill of Colville basin, and the subsurface load of crustal root very well define the flexure of the lithosphere underneath the Arctic Alaska microplate. An additional subsurface dynamic load like mantle pull is not required in the northern Alaska region to support the bending forces.

In contrast, Nunn et al. (1987) show that a subsurface load is needed to bend the lithosphere to create desirable deflection in the Colville basin. There are several reasons for disagreement; they used a simple 2D modeling approach and assumed that the geometry of the Colville basin is relatively uniform. However, a detailed analysis of geometry reveals that the basin depth varies abruptly adjacent to the Brooks Range (see Figure 1). Since the basin geometry is non-uniform, a more robust 3D modeling technique that accounts for geometrical variations in the basin was needed to accurately model the basin flexure. Next, their flexure results estimate high elastic thickness values, which assume a deficit of the load compensated by replacing crustal material with the mantle. The elastic strength of the lithosphere dissipates at the crust-mantle boundary, with exceptions to the cratonic regions (Maggi et al., 2000). Although this view is debated from the rheological viewpoint, it is considered a valid explanation for various tectonic settings, for example, a rifted passive margin undergoing subsequent thrusting (Watts & Burov, 2003). Since Arctic Alaska microplate also underwent thrusting subsequent with rifting, it suggests that the elastic strength would most likely be associated with the crust, with little/no influence from the mantle in this region. Nunn et al. (1987) used the top of the Lower Cretaceous Pebble Shale to reconstruct the geometry basin, whereas we used LCU unconformity as the foreland basin depth indicator. We show that the wavelength of the Colville basin is very well correlated with the size of the Brooks Range along with associated crustal root that is proportional to the size of the orogen. It is not suitable to invoke an additional subsurface force that would cause the deflection of the Colville basin.

4.4. Gravity and Flexural Support

Orogenic wedge and adjacent foreland basin show positive and negative values of free air anomaly in response to the flexed lithosphere during a mountain building process (Karner & Watts, 1983; L. Royden & Karner, 1984). Obtained free air anomaly from geological and geophysical models can be compared to the observed anomaly to evaluate the modeling results. We examined fidelity of the flexural model of Arctic Alaska from modeled gravity and free air anomalies. To this purpose, we calculate FAA in Arctic Alaska using two different data sources. One is based on the seismic Moho depth provided by Torne et al., 2020, and the other from our flexural model (Figures 8 and 9). The estimated FAA from the flexural model shows that the Brooks Range is characterized by 150 mGal positive value representing a thick crust, and the adjacent Colville basin shows a decrease in anomalies close to -50 mGal (Figures 7 and 8). Correlation between the observed and predicted FAA shows that our FAA model significantly well characterizes the Colville basin and the Brooks Range signals. The northern portion of the cross-sections that spans over 200 km shows a perfect fit to the observed FAA, and the southern portion shows a relatively good correlation along the Brooks Range thrust belt. Calculations of FAA derived from seismic Moho (see figures 7 and 8) has a good overall correlation with the observed anomalies. There is a significant mismatch over the basin, about 40 mGal, in which the higher values are probably due to the ignored mass deficit. Modeled FAA signal in Arctic Alaska supports and validates our flexural model of the Colville foreland basin. The FAA calculated by the flexural deflection model is very well correlated with observed FAA anomalies with a maximum misfit of only 27 mGal. Since the FAA anomalies derived from the deflection model fit well to the observed data, 13-16 km of estimated effective elastic thickness is an accurate representation of elastic strength of the Arctic Alaska lithosphere.

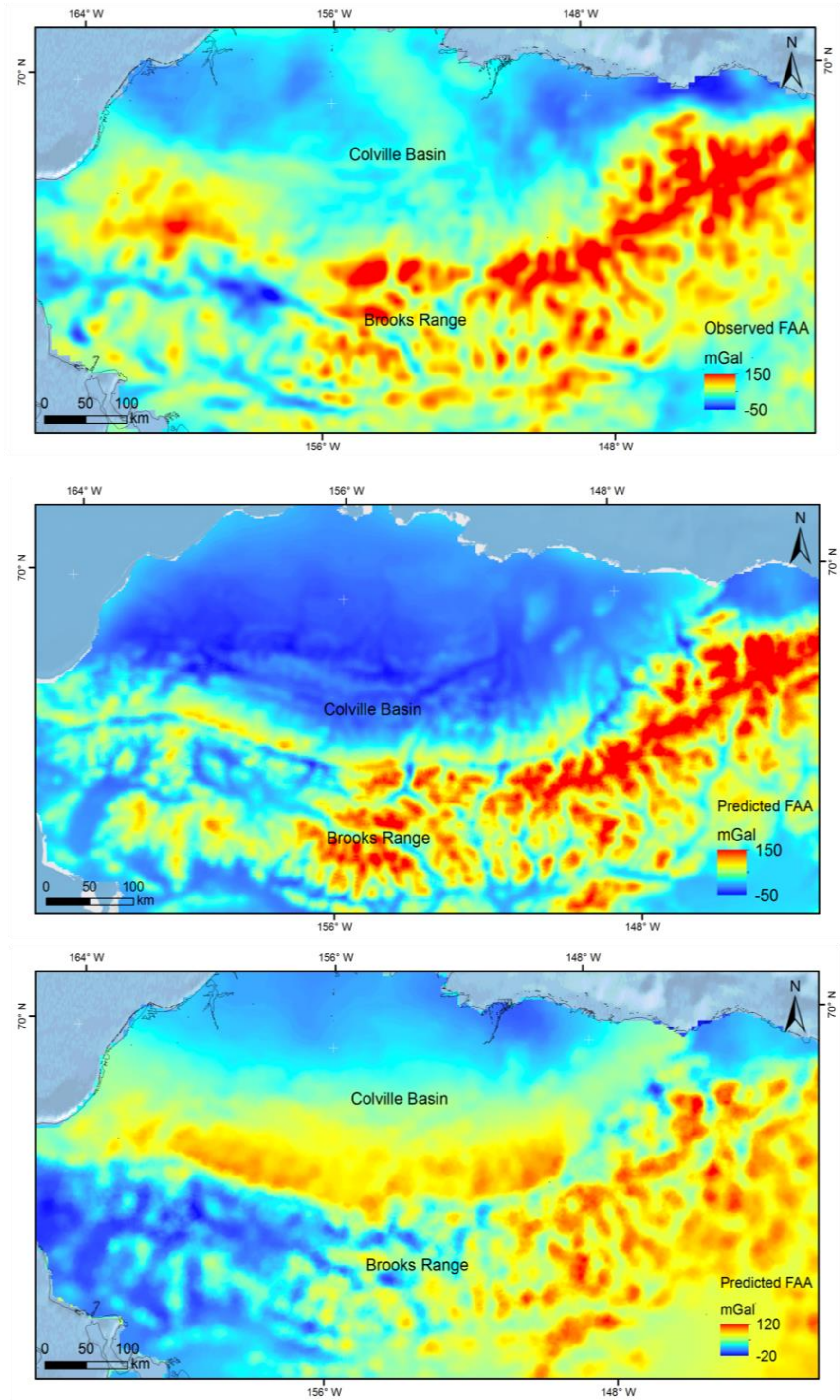

Figure 8. (a) observed, (b) predicted from the flexural model, and (c) predicted from Moho FAA. The Brooks Range is characterized by significantly closer to zero anomalies (yellow) in the central thrust belt except for high values (red) where the belt extends further into the present-day shelf. Colville basin has a typical foreland basin low anomaly response (blue color).

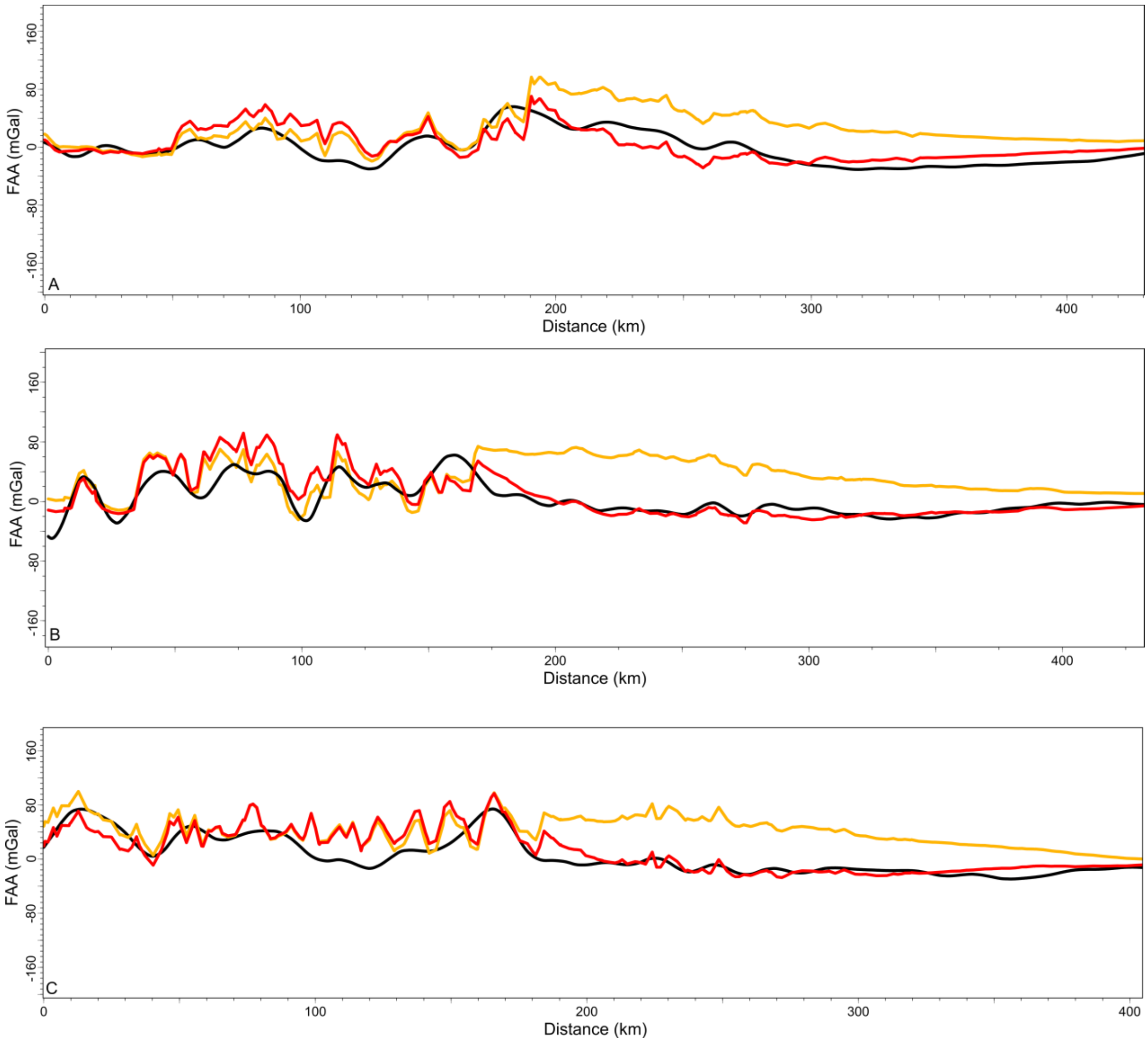

Figure 9. A comparison between observed FAA (black Curve; Bonvalot et al., 2012) with calculated FAA from seismic Moho (orange) (Torne et al., 2020) and deflection model (red, this study) along the sections A, B, and C. Location of sections are shown in Figure 1.

4.5. Seismogenic Layer in the Brooks Range

Earthquakes mostly occur in the uppermost part of the brittle and competent layer of the crustal lithosphere, supporting the elastic stresses. The seismogenic layer is usually about < 20 km, except the subduction zones where deep earthquakes (~40 km) can also occur. The strength of a continental lithosphere is likely contained within the seismogenic layer (Maggi et al., 2000). Earthquakes may extend into deeper depth, into the brittle zone of the sub-crustal mantle on major faults, in regions of high curvature or high bending stresses (Watts & Burov, 2003). In southern Alaska, near the Pacific subduction zone, the reported seismogenic layer thickness is 25 km (Walton et al., 2019). On the other hand, until recently, mapping and characterization of active faults in the northern Alaska region have been limited, mostly due to lack of geological mapping and harsh climate conditions (Gaudreau et al., 2019; Gibbons et al., 2020).

In northern Alaska, earthquake monitoring began as early as the 1970s (Estabrook et al., 1988), with moderate-sized earthquakes detected every few years. Interestingly, the recent deployment of seismic networks, notably, Earthscope USArray (Ruppert & West, 2020), has shown an increase in recorded earthquake activity, particularly in the northeastern Brooks Range. This increase in seismicity has redrawn interest in seismological studies in northern Alaska (Gaudreau et al., 2019; Gibbons et al., 2020; Xu et al., 2020). In our study area, the observed seismicity is summarized in Figures 10 and 11, which shows the distribution, magnitude, and frequency histogram of a total of 752 seismic events (1960 to present) with a large magnitude ($\geq 4\ to \leq 6.3$). In northern Alaska, the maximum number of earthquake frequency dissipates at depths between 10 and 15 km. Seismological studies in this region indicate that the driving forces of tectonic activity mainly result from deformation associated with far-field stresses originating from mantle flow and the northward movement of tectonic Yakutat block due to subduction of Pacific plate at the southern Alaskan margin. (Berg et al., 2020; Mazzotti et al., 2013; Mazzotti & Hyndman, 2002). These evidences indicate presence of a strong mantle that serves as a guiding block in the northern Alaska region for the strain transmission from the south toward north. Consequently, most of these studies conclude the presence of a strong and cold lithosphere.

On the scale of entire Alaska and Canada, mechanically weak zones in the lithosphere and high heat flow is also indicated (Mazzotti & Hyndman, 2002). Furthermore, the flexural model of this study indicates weakness in the northern part of the Alaska lithosphere. To explain these contrasting rheological observations, we again resort to the decoupling phenomena. We assert that brittle crust and mantle decoupling is the only plausible explanation of the weak elastic lithosphere with strong mantle rheology. This view is also supported by the observation of earthquakes limited to the brittle part of the crust in the northern Alaska region. It implies that the elasticity diminishes below this depth in the crust, which validates our computed 13-16 km elastic thickness from the flexure model. For a lithospheric plate whose strength comes from subsurface mantle forces as predicted previously (Nunn et al., 1987), we would expect the frequent occurrence of deep earthquakes in Arctic Alaska. However, there are few sporadically recorded earthquakes in this region at a depth greater than 60 km. The second peak of observed earthquakes at 40-45 km is more likely correlated to the Moho boundary. Our results show that induced stresses from southern Alaska have less/no influence on the lithosphere's mechanical strength in northern Alaska and the Colville basin. These tectonic stresses might be localized within the substantial portion of the mantle and thus only provide means of strain transfer to direct an overall northward plate motion.

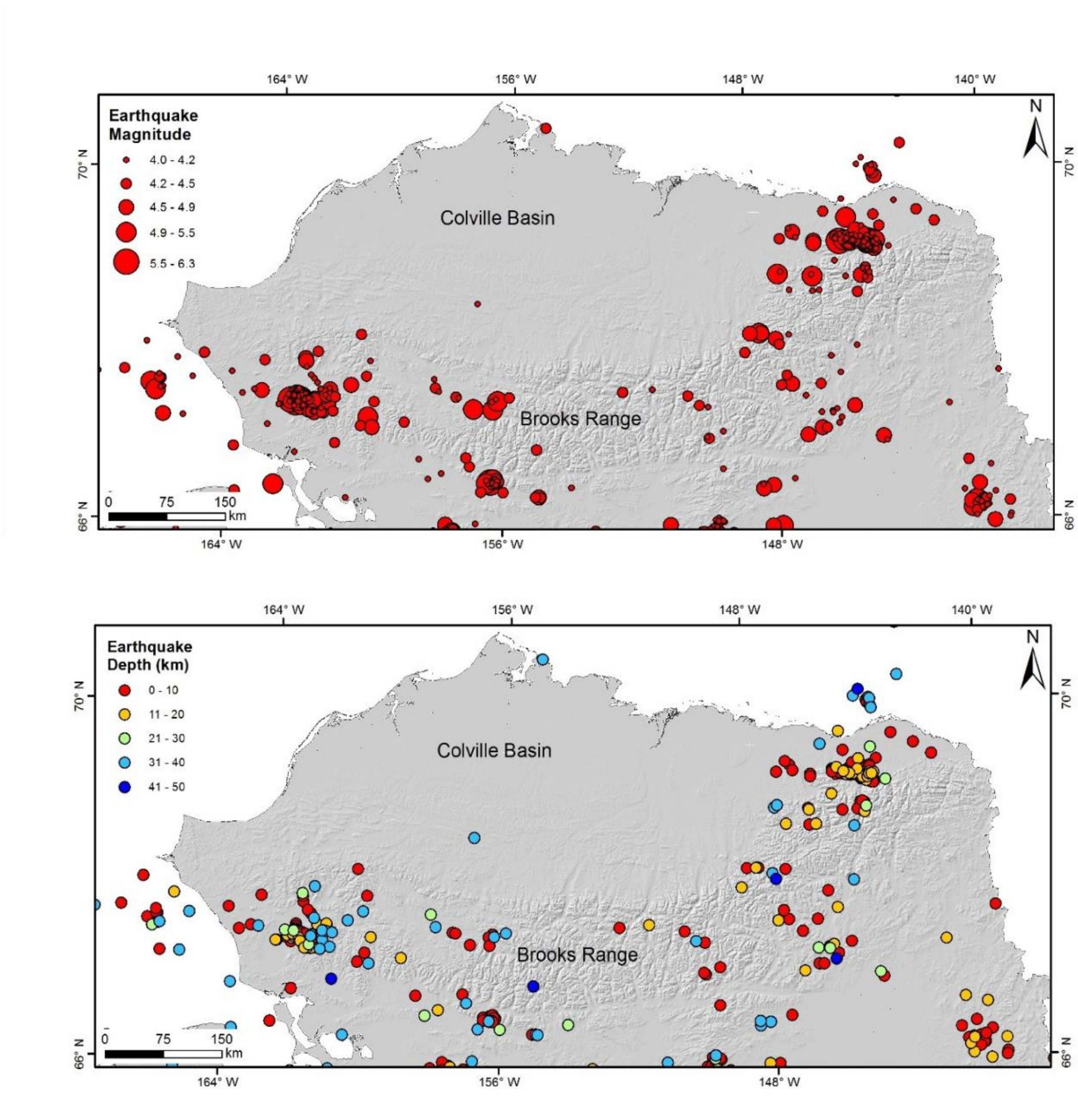

Figure 10. The upper panel shows locations of earthquakes with their corresponding depth. The lower panel shows the corresponding magnitude of earthquakes in the Brooks Range area. Data collected from IRIS Catalog using Zmap software

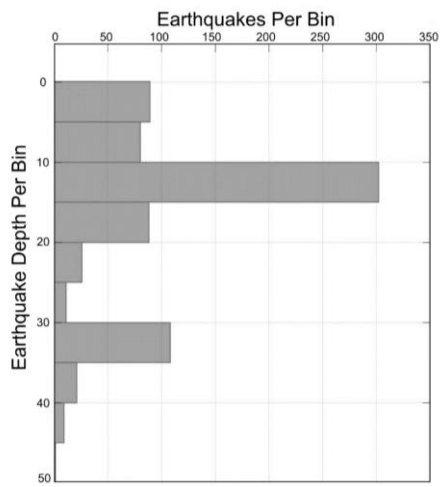

Figure 11. Frequency distribution chart showing the maximum depth of most frequent earthquakes in the Brooks Range and Colville basin dissipates at 20 km depth.

5. Conclusions

The elastic thickness of the lithosphere is an essential feature of plate geomechanics. Our simple 3D flexural modeling results quantitatively evaluate the elastic properties of the lithosphere in the northern Alaska region. The flexural model of the Colville basin with 13-16 km thickness and a load of crustal root with a scaling factor of 3.4-4.5 times of the topography provides a best-fitting model to present-day geometry of the Colville basin with 3% of average misfit error over the basin. Frequent earthquakes dissipate near 20 km depth, where the crust behaves aseismic and does not transmit significant stresses below this depth. Since the Brooks Range and the Colville basin sediment loads provide an accurate deflection of the Colville basin, there is no need to invoke an additional subsurface dynamic load as inferred previously. A comparison free air anomaly between observed, obtained from the flexural model, and derived from the Moho boundary shows an excellent correlation for the wedge and the basin area. The maximum error is only 27 mGal.

Acknowledgments

The authors thank Dr. Hejun Zhu and Dr. Robert Stern for their constructive feedback.

Data Availability Statement

No new data has been utilized in this research. The data for flexural model is available through (Bird & Houseknecht, 2011). Moho boundary dataset is available in (Torne et al., 2020). Free-air surface gravity anomalies dataset is available from (Bonvalot et al., 2012). The code to model the flexure is available from (Pirouz et al., 2017).

References

Afonso, J. C., & Ranalli, G. (2004). Crustal and mantle strengths in continental lithosphere: Is the jelly sandwich model obsolete? Tectonophysics, 394(3), 221–232. https://doi.org/10.1016/j.tecto.2004.08.006

Angrand, P., Ford, M., & Watts, A. B. (2018). Lateral Variations in Foreland Flexure of a Rifted Continental Margin: The Aquitaine Basin (SW France). Tectonics, 37(2), 430–449. https://doi.org/10.1002/2017TC004670

Arnaiz-Rodríguez, M. S., Álvarez Hostos, J. C., & Audemard, F. (2020). LIFFE: Lithospheric flexure with finite elements. Computers & Geosciences, 140, 104483. https://doi.org/10.1016/j.cageo.2020.104483

Beaumont, C. (1981). Foreland basins. Geophysical Journal International, 65(2), 291–329. https://doi.org/10.1111/j.1365-246X.1981.tb02715.x

Bechtel, T. D., Forsyth, D. W., Sharpton, V. L., & Grieve, R. A. F. (1990). Variations in effective elastic thickness of the North American lithosphere. Nature, 343(6259), 636–638. https://doi.org/10.1038/343636a0

Berg, E. M., Lin, F.-C., Allam, A., Schulte-Pelkum, V., Ward, K. M., & Shen, W. (2020). Shear Velocity Model of Alaska Via Joint Inversion of Rayleigh Wave Ellipticity, Phase Velocities, and Receiver Functions Across the Alaska Transportable Array. Journal of Geophysical Research: Solid Earth, 125(2), e2019JB018582. https://doi.org/10.1029/2019JB018582

Bird, K. J. (2001). Framework Geology, Petroleum Systems, and Play Concepts of the National Petroleum Reserve – Alaska. https://doi.org/10.2110/cor.01.01.0005

Bird, K. J., & Houseknecht, D. W. (2011). Chapter 32 Geology and petroleum potential of the Arctic Alaska petroleum province. Geological Society, London, Memoirs, 35(1), 485–499. https://doi.org/10.1144/M35.32

Bird, K. J., & Molenaar, C. M. (1992). The North Slope Foreland Basin, Alaska: Chapter 13. 136, 363–393.

Bonvalot, S., Balmino, G., Briais, A., Kuhn, M., Peyrefitte, A., Vales, N., Biancale, R., Gabalda, G., & Reinquin, F. (2012). World Gravity Map: A set of global complete spherical Bouguer and isostatic anomaly maps and grids. 14, 11091.

Box, S. E. (1985). Early Cretaceous Orogenic Belt in Northwestern Alaska: Inernal Organization, Lateral Extent, and Tectonic Interpretation. http://archives.datapages.com/data/circ_pac/1/137_b.htm

Braitenberg, C., Ebbing, J., & Goetze, H. (2002). Inverse modelling of elastic thickness by convolution method – the eastern Alps as a case example. https://doi.org/10.1016/S0012-821X(02)00793-8

Brown, C. D., & Phillips, R. J. (2000). Crust-mantle decoupling by flexure of continental lithosphere. Journal of Geophysical Research: Solid Earth, 105(B6), 13221–13237. https://doi.org/10.1029/2000JB900069

Burov, E B. (2006). The long-term strength of continental lithosphere: "Jelly sandwich" or "crème brûlée"? GSA TODAY, 7.

Burov, Evgene B., & Diament, M. (1995). The effective elastic thickness (T e) of continental lithosphere: What does it really mean? Journal of Geophysical Research: Solid Earth, 100(B3), 3905–3927. https://doi.org/10.1029/94JB02770

Cattin, R., Martelet, G., Henry, P., Avouac, J. P., Diament, M., & Shakya, T. R. (2001). Gravity anomalies, crustal structure and thermo-mechanical support of the Himalaya of Central Nepal. Geophysical Journal International, 147(2), 381–392. https://doi.org/10.1046/j.0956-540x.2001.01541.x

Cole, F., Bird, K. J., Toro, J., Roure, F., O'Sullivan, P. B., Pawlewicz, M., & Howelll, D. G. (1997). An integrated model for the tectonic development of the frontal Brooks Range and Colville Basin 250 km west of the Trans-Alaska Crustal Transect. Journal of Geophysical Research: Solid Earth, 102(B9), 20685–20708. https://doi.org/10.1029/96JB03670

Curry, M. E., van der Beek, P., Huismans, R. S., Wolf, S. G., & Muñoz, J.-A. (2019). Evolving paleotopography and lithospheric flexure of the Pyrenean Orogen from 3D flexural modeling and basin analysis. Earth and Planetary Science Letters, 515, 26–37. https://doi.org/10.1016/j.epsl.2019.03.009

DeCelles, P. G. (2012). Foreland Basin Systems Revisited: Variations in Response to Tectonic Settings. In Tectonics of Sedimentary Basins (pp. 405–426). John Wiley & Sons, Ltd. https://doi.org/10.1002/9781444347166.ch20

Decker, P. L. (2007). Brookian sequence stratigraphic correlations, Umiat Field to Milne Point Field, west-central North Slope, Alaska (PIR 2007-2; p. PIR 2007-2). Alaska Division of Geological & Geophysical Surveys. https://doi.org/10.14509/15758

Desegaulx, P., Kooi, H., & Cloetingh, S. (1991). Consequences of foreland basin development on thinned continental lithosphere: Application to the Aquitaine basin (SW France). Earth and Planetary Science Letters, 106(1), 116–132. https://doi.org/10.1016/0012-821X(91)90067-R

Embry, A. F. (1990). Geological and geophysical evidence in support of the hypothesis of anticlockwise rotation of northern Alaska. Marine Geology, 93, 317–329. https://doi.org/10.1016/0025-3227(90)90090-7

Eshagh, M., Tenzer, R., & Eshagh, M. (2020). Elastic thickness of the Iranian lithosphere from gravity and seismic data. Tectonophysics, 774, 228186. https://doi.org/10.1016/j.tecto.2019.228186

Estabrook, C. H., Stone, D. B., & Davies, J. N. (1988). Seismotectonics of northern Alaska. Journal of Geophysical Research: Solid Earth, 93(B10), 12026–12040. https://doi.org/10.1029/JB093iB10p12026

Forsyth, D. W. (1985). Subsurface loading and estimates of the flexural rigidity of continental lithosphere. Journal of Geophysical Research: Solid Earth, 90(B14), 12623–12632. https://doi.org/10.1029/JB090iB14p12623

Fosdick, J. C., Graham, S. A., & Hilley, G. E. (2014). Influence of attenuated lithosphere and sediment loading on flexure of the deep-water Magallanes retroarc foreland basin, Southern Andes. Tectonics, 33(12), 2505–2525. https://doi.org/10.1002/2014TC003684

Fuis, Gary S., Moore, T. E., Plafker, G., Brocher, T. M., Fisher, M. A., Mooney, W. D., Nokleberg, W. J., Page, R. A., Beaudoin, B. C., Christensen, N. I., Levander, A. R., Lutter, W. J., Saltus, R. W., & Ruppert, N. A. (2008). Trans-Alaska Crustal Transect and continental evolution involving subduction underplating and synchronous foreland thrusting. Geology, 36(3), 267–270. https://doi.org/10.1130/G24257A.1

Fuis, G.S., Murphy, J. M., Lutter, W. J., Moore, T. E., Bird, K. J., & Christensen, N. I. (1997). Deep seismic structure and tectonics of northern Alaska: Crustal-scale duplexing with deformation extending into the upper mantle. Journal of Geophysical Research B: Solid Earth, 102(B9), 24.

Garcia-Castellanos, D. (2002). Interplay between lithospheric flexure and river transport in foreland basins. Basin Research, 14(2), 89–104. https://doi.org/10.1046/j.1365-2117.2002.00174.x

Garcia-Castellanos, D., Fernàndez, M., & Torne, M. (1997). Numerical modeling of foreland basin formation: A program relating thrusting, flexure, sediment geometry and lithosphere rheology. Computers & Geosciences, 23(9), 993–1003. https://doi.org/10.1016/S0098-3004(97)00057-5

Gaudreau, É., Nissen, E. K., Bergman, E. A., Benz, H. M., Tan, F., & Karasözen, E. (2019). The August 2018 Kaktovik Earthquakes: Active Tectonics in Northeastern Alaska Revealed With InSAR and Seismology. Geophysical Research Letters, 46(24), 14412–14420. https://doi.org/10.1029/2019GL085651

Gibbons, S. J., Ruppert, N. A., Karasözen, E., Aderhold, K., & Dickson, I. (2020). Resolving Northern Alaska Earthquake Sequences Using the Transportable Array and Probabilistic Location Methods. Seismological Research Letters. https://doi.org/10.1785/0220200142

Grantz, A., & May, S. D. (1982). Rifting history and structural development of the continental margin north of Alaska. In American Association of Petroleum Geologists (Ed.), M 34: Studies in continental margin geology (pp. 77–100).

American Association of Petroleum Geologists; USGS Publications Warehouse. http://pubs.er.usgs.gov/publication/70186628

Grantz, A., May, S. D., & Hart, P. E. (1994). Geology of the Arctic continental margin of Alaska. In G. Plafker & H. C. Berg (Eds.), The Geology of Alaska (pp. 17–48). Geological Society of America. https://doi.org/10.1130/DNAG-GNA-G1.17

Haddad, D., & Watts, A. B. (1999). Subsidence history, gravity anomalies, and flexure of the northeast Australian margin in Papua New Guinea. Tectonics, 18(5), 827–842. https://doi.org/10.1029/1999TC900009

Houseknecht, D. W. (2019). Chapter 18—Evolution of the Arctic Alaska Sedimentary Basin. In A. D. Miall (Ed.), The Sedimentary Basins of the United States and Canada (Second Edition) (pp. 719–745). Elsevier. https://doi.org/10.1016/B978-0-444-63895-3.00018-8

Houseknecht, D. W., Bird, K. J., & Schenk, C. J. (2009). Seismic analysis of clinoform depositional sequences and shelf-margin trajectories in Lower Cretaceous (Albian) strata, Alaska North Slope. Basin Research, 21(5), 644654. https://doi.org/10.1111/j.1365-2117.2008.00392.x

Houseknecht, D. W., & Wartes, M. A. (2013). Clinoform deposition across a boundary between orogenic front and foredeep—An example from the Lower Cretaceous in Arctic Alaska. Terra Nova, 25(3), 206–211. https://doi.org/10.1111/ter.12024

Hubbard, R. J., Edrich, S. P., & Peter Rattey, R. (1987). Geologic evolution and hydrocarbon habitat of the ‘Arctic Alaska Microplate.’ Marine and Petroleum Geology, 4(1), 2–34. https://doi.org/10.1016/0264-8172(87)90019-5

Jackson, J. (2002). Strength of the continental lithosphere: Time to abandon the jelly sandwich? GSA TODAY, 6.

Kaban, M. K., Chen, B., Tesauro, M., Petrunin, A. G., Khrepy, S. E., & Al-Arifi, N. (2018). Reconsidering Effective Elastic Thickness Estimates by Incorporating the Effect of Sediments: A Case Study for Europe. Geophysical Research Letters, 45(18), 9523–9532. https://doi.org/10.1029/2018GL079732

Karner, G. D., & Watts, A. B. (1983). Gravity anomalies and flexure of the lithosphere at mountain ranges. Journal of Geophysical Research: Solid Earth, 88(B12), 10449–10477. https://doi.org/10.1029/JB088iB12p10449

Kirby, J. F., & Swain, C. J. (2009). A reassessment of spectral Te estimation in continental interiors: The case of North America. Journal of Geophysical Research: Solid Earth, 114(B8). https://doi.org/10.1029/2009JB006356

Kirby, J. F., & Swain, C. J. (2011). Improving the spatial resolution of effective elastic thickness estimation with the fan wavelet transform. Computers & Geosciences, 37(9), 1345–1354. https://doi.org/10.1016/j.cageo.2010.10.008

Lin, A. T., & Watts, A. B. (2002). Origin of the West Taiwan basin by orogenic loading and flexure of a rifted continental margin. Journal of Geophysical Research: Solid Earth, 107(B9), ETG 2-1-ETG 2-19. https://doi.org/10.1029/2001JB000669

Lyon-Caen, H., & Molnar, P. (1983). Constraints on the structure of the Himalaya from an analysis of gravity anomalies and a flexural model of the lithosphere. Journal of Geophysical Research: Solid Earth, 88(B10), 8171–8191. https://doi.org/10.1029/JB088iB10p08171

Maggi, A., Jackson, J. A., McKenzie, D., & Priestley, K. (2000). Earthquake focal depths, effective elastic thickness, and the strength of the continental lithosphere. Geology, 28(6), 495–498. https://doi.org/10.1130/0091-7613(2000)28<495:EFDEET>2.0.CO;2

Mayfield, C. F., Tailleur, I. L., & Ellersieck, I. (1983). Stratigraphy, structure, and palinspastic synthesis of the western Brooks Range, northwestern Alaska (USGS Numbered Series No. 83–779; Open-File Report). U.S. Geological Survey,. http://pubs.er.usgs.gov/publication/ofr83779

Mazzotti, Stéphane, & Hyndman, R. D. (2002). Yakutat collision and strain transfer across the northern Canadian Cordillera. Geology, 30(6), 495–498. https://doi.org/10.1130/0091-7613(2002)030<0495:YCASTA>2.0.CO;2

Mazzotti, Stephane, Leonard, L. J., Hyndman, R. D., & Cassidy, J. F. (2013). Tectonics, Dynamics, and Seismic Hazard in the Canada-Alaska Cordillera. In J. T. Freymueller, P. J. Haeussler, R. L. Wesson, & G. Ekström (Eds.), Geophysical Monograph Series (pp. 297–319). American Geophysical Union. https://doi.org/10.1029/179GM17

McKenzie, D. (2010). The influence of dynamically supported topography on estimates of Te. Earth and Planetary Science Letters, 295(1), 127–138. https://doi.org/10.1016/j.epsl.2010.03.033

McKenzie, D., & Fairhead, D. (1997). Estimates of the effective elastic thickness of the continental lithosphere from Bouguer and free air gravity anomalies. Journal of Geophysical Research: Solid Earth, 102(B12), 27523–27552. https://doi.org/10.1029/97JB02481

Miller, M. S., O’Driscoll, L. J., Porritt, R. W., & Roeske, S. M. (2018). Multiscale crustal architecture of Alaska inferred from P receiver functions. Lithosphere, 10(2), 267–278. https://doi.org/10.1130/L701.1

Miller, T. P. (1994). Pre-Cenozoic plutonic rocks in mainland Alaska. In G. Plafker & H. C. Berg (Eds.), The Geology of Alaska (pp. 535–554). Geological Society of America. https://doi.org/10.1130/DNAG-GNA-G1.535

Moore, T. E., & Box, S. E. (2016). Age, distribution and style of deformation in Alaska north of 60°N: Implications for assembly of Alaska. Tectonophysics, 691, 133–170. https://doi.org/10.1016/j.tecto.2016.06.025

Moore, T. E., Potter, C. J., O’Sullivan, P. B., Shelton, K. L., & Underwood, M. B. (2004). Two stages of deformation and fluid migration in the central Brooks Range fold-and-thrust belt. In AAPG Bulletin (Vol. 1, p. 20).

Moore, T. E., Wallace, W. K., Bird, K. J., Karl, S. M., Mull, C. G., & Dillon, J. T. (1994). Geology of northern Alaska. In G. Plafker & H. C. Berg (Eds.), The Geology of Alaska (pp. 49–140). Geological Society of America. https://doi.org/10.1130/DNAG-GNA-G1.49

Mull, C. G. (1982). Tectonic Evolution and Structural Style of the Brooks Range, Alaska: An Illustrated Summary. http://archives.datapages.com/data/rmag/GeoStudCordV1_82/mull.htm

Nunn, J. A., Czerniak, M., & Pilger, R. H. (1987). Constraints on the structure of Brooks Range and Colville Basin, northern Alaska, from flexure and gravity analysis. Tectonics, 6(5), 603–617. https://doi.org/10.1029/TC006i005p00603

Patton, W. W., & Box, S. E. (1989). Tectonic setting of the Yukon-Koyukuk Basin and its borderlands, western Alaska. Journal of Geophysical Research: Solid Earth, 94(B11), 15807–15820. https://doi.org/10.1029/JB094iB11p15807

Patton, W. W., Box, Stephen. E., & Grybeck, D. J. (1994). Ophiolites and other mafic-ultramafic complexes in Alaska. In G. Plafker & H. C. Berg (Eds.), The Geology of Alaska (pp. 671–686). Geological Society of America. https://doi.org/10.1130/DNAG-GNA-G1.671

Pirouz, M., Avouac, J.-P., Gualandi, A., Hassanzadeh, J., & Sternai, P. (2017). Flexural bending of the Zagros foreland basin. Geophysical Journal International, 210(3), 1659–1680. https://doi.org/10.1093/gji/ggx252

Pirouz, M., Avouac, J.-P., Gualandi, A., Quddusi, M. H., & Huang, W. (2020). New Versus Conventional Approach for Modeling Flexure of Foreland Basins (No. EGU2020-13016). EGU2020. Copernicus Meetings. https://doi.org/10.5194/egusphere-egu2020-13016

Plafker, G., & Berg, H. C. (1994). Overview of the geology and tectonic evolution of Alaska. In The Geology of Alaska (pp. 989–1021). Geological Society of America. https://doi.org/10.1130/DNAG-GNA-G1.989

Royden, L., & Karner, G. D. (1984). Flexure of Lithosphere Beneath Apennine and Carpathian Foredeep Basins: Evidence for an Insufficient Topographic Load. AAPG Bulletin, 68(6), 704–712.

Ruppert, N. A., & West, M. E. (2020). The Impact of USArray on Earthquake Monitoring in Alaska. Seismological Research Letters, 91(2A), 601–610. https://doi.org/10.1785/0220190227

Simpson, G. (2017). Practical finite element modeling in earth science using Matlab. John Wiley & Sons.

Stier, N. E., Connors, C. D., & Houseknecht, D. W. (2014). Influence of the Kingak Shale ultimate shelf margin on frontal structures of the Brooks Range in the National Petroleum Reserve in Alaska (USGS Numbered Series No. 2014–5056; Scientific Investigations Report, p. 20). U.S. Geological Survey. http://pubs.er.usgs.gov/publication/sir20145056

Sweeney, J. F. (1985). Comments about the age of the Canada Basin. Tectonophysics, 114(1), 1–10. https://doi.org/10.1016/0040-1951(85)90004-6

Tesauro, M., Audet, P., Kaban, M. K., Bürgmann, R., & Cloetingh, S. (2012). The effective elastic thickness of the continental lithosphere: Comparison between rheological and inverse approaches. Geochemistry, Geophysics, Geosystems, 13(9). https://doi.org/10.1029/2012GC004162

Till, A. B. (2016). A synthesis of Jurassic and Early Cretaceous crustal evolution along the southern margin of the Arctic Alaska–Chukotka microplate and implications for defining tectonic boundaries active during opening of Arctic Ocean basins. Lithosphere, 8(3), 219–237. https://doi.org/10.1130/L471.1

Torne, M., Jiménez–Munt, I., Vergés, J., Fernàndez, M., Carballo, A., & Jadamec, M. (2020). Regional crustal and lithospheric thickness model for Alaska, the Chukchi shelf, and the inner and outer bering shelves. Geophysical Journal International, 220(1), 522–540. https://doi.org/10.1093/gji/ggz424

Turcotte, D. L., & Schubert, G. (2002). Geodynamics—2nd Edition. https://doi.org/10.2277/0521661862

Wallace, W. K., Moore, T. E., & Plafker, G. (1997). Multistory duplexes with forward dipping roofs, north central Brooks Range, Alaska. Journal of Geophysical Research: Solid Earth, 102(B9), 20773–20796. https://doi.org/10.1029/96JB02682

Walton, M. A. L., Roland, E. C., Walter, J. I., Gulick, S. P. S., & Dotray, P. J. (2019). Seismic velocity structure across the 2013 Craig, Alaska rupture from aftershock tomography: Implications for seismogenic conditions. Earth and Planetary Science Letters, 507, 94–104. https://doi.org/10.1016/j.epsl.2018.11.021

Watts, A. B. (1992). The effective elastic thickness of the lithosphere and the evolution of foreland basins. Basin Research, 4(3–4), 169–178. https://doi.org/10.1111/j.1365-2117.1992.tb00043.x

Watts, A. B. (2001). Isostasy and flexure of the lithosphere. Cambridge University Press.

Watts, A. B., & Burov, E. B. (2003). Lithospheric strength and its relationship to the elastic and seismogenic layer thickness. Earth and Planetary Science Letters, 213(1), 113–131. https://doi.org/10.1016/S0012-821X(03)00289-9

Wiemer, S. (2001). A Software Package to Analyze Seismicity: ZMAP. Seismological Research Letters, 72(3), 373–382. https://doi.org/10.1785/gssrl.72.3.373

Wienecke, S., Braitenberg, C., & Götze, H.-J. (2007). A new analytical solution estimating the flexural rigidity in the Central Andes. Geophysical Journal International, 169(3), 789–794. https://doi.org/10.1111/j.1365-246X.2007.03396.x

Xu, G., Xu, C., Wen, Y., Xiong, W., & Valkaniotis, S. (2020). The Complexity of the 2018 Kaktovik Earthquake Sequence in the Northeast of the Brooks Range, Alaska. Geophysical Research Letters, 47(19), e2020GL088012. https://doi.org/10.1029/2020GL088012

Supporting Information for

Flexural Modeling of the Colville Foreland Basin, Northern Alaska

M.H. Quddusi[1], M. Pirouz[1]

[1]Department of Geosciences, The University of Texas at Dallas, Richardson, Texas, USA

Contents of this file

Introduction

The following supporting information includes **Text S1**, which discusses the equations to calculate deflection parameters. **Text S2**, provides information for calculating free-air anomalies from the flexural model and Moho boundary data. **Figure S1**, shows Root mean square error (RMSE) between the observed and predicted FAA. **Figure S2** shows location of sections for Figure S2 and S3. **Figure S3** and **Figure S4** shows cross sections of flexural deflection model and FAA calculation, respectively. **Figure S5** shows density distribution versus depth in the Colville foreland basin for calculation of vertical density variation. **Figure S6** shows the misfit map of flexural deflection model.

Text S1. Deflection Calculation:

The flexure (ω) of a thin elastic plate is calculated by following three distinct solutions (Wienecke et al., 2007):

$$1.\ \omega = \frac{P}{8(\rho mantle - \ \rho crust)g\beta^2}$$

$$2.\ \omega(x,y) = \frac{P}{2\pi\beta^2(\rho mantle - \rho crust)g} \times \left\{ \begin{array}{c} \frac{(r_{x,y})^2}{2^2} \times ln(r_{x,y}) - \frac{(r_{x,y})^6}{2^2.4^2.6^2} \times \left(ln(r_{x,y}) - \frac{5}{6}\right) + \cdots \\ + \frac{\pi}{4}\left(1 - \frac{(r_{x,y})^2}{2^2.4^2} + \frac{(r_{x,y})^8}{2^2.4^2.6^2.8^2}\right) \\ \ldots - 1.1159 \times \left(\frac{(r_{x,y})^2}{2^2} - \frac{(r_{x,y})^6}{2^2.4^2.6^2} + \cdots\right) \end{array} \right\}$$

$$3.\ \omega(x,y) = \frac{P}{2\pi\beta^2(\rho mantle - \rho crust)g} \times \sqrt{\frac{\pi}{2}} \frac{e^{-(x,y)\sqrt{1/2}}}{\sqrt{(r_{x,y})}}$$

$$\times \left\{ sin\left[(r_{x,y}) \sqrt{\frac{1}{2} + \frac{\pi}{8}} \right] - \frac{1}{8(r_{x,y})} sin\left[(r_{x,y}) \sqrt{\frac{1}{2} + \frac{3\pi}{8}} \right] + \cdots \right\}$$

Here β is the flexural parameter, P is the applied load and $r_{x,y}$ is the radial distance from the point of origin. The first solution calculates the maximum depth of deflection; the second solution accounts for log-function where $r_{x,y} \leq 2\beta$ and the third solution accounts for sine-function where $r_{x,y} \geq 2\beta$. The log-function is only valid for small values of the radius $r_{x,y}$, whereas the deflection values produced by the sine-function are underestimated for smaller values of the radius $r_{x,y}$. The analytical solution is derived by using all three methods by using the expression $r_{x,y} = 2\beta$ for the change in the function from log to sine. To consider point load distribution, the Green's function is used which is simply given by dividing P by the ω. The Green's function for a point load represents a two-dimensional (2-D) radial cross section in the *r-z* plane (*r* is the radial coordinate position) across a radially symmetric flexural basin, normalized by the magnitude of the load. By convolving the Green's function with P, the deflection due to the distributed loads can be calculated (Pirouz et.al., 2017).

Text S2. Free Air Anomaly (FAA) calculation

FAA calculation is done for (1) flexure modeling results and (2) Moho data, which is described by following equations.

$$\Delta g_{(x,y)} = 0.0419(\rho_c - \rho_m)(Moho_{(x,y)} - T_c)$$

$$\delta gB_{(x,y)} = 0.0419\left[(\rho_c - \rho_{air})\left(Topo_{(x,y)} - T_c\right) + (\rho_b - \rho_c)\left(Basin_{(x,y)}\right)\right]$$

$$\Delta g_{elev_{(x,y)}} = \Delta g_{(x,y)} + \delta gB_{(x,y)}$$

Here equations 1, 2, and 3 calculate Bouguer anomaly ($\Delta g_{(x,y)}$), Bouguer Correction ($\delta gB_{(x,y)}$) and Free-air Anomaly ($\Delta g_{elev_{(x,y)}}$), where ρ_b, ρ_c and ρ_m are basin, crust and mantle density, respectively. The depth of basin and Moho is given by $Basin_{(x,y)}$ and $Moho_{(x,y)}$, topography is $Topo_{(x,y)}$, and undeformed crustal thickness is given by T_c (Pirouz et al., 2017).

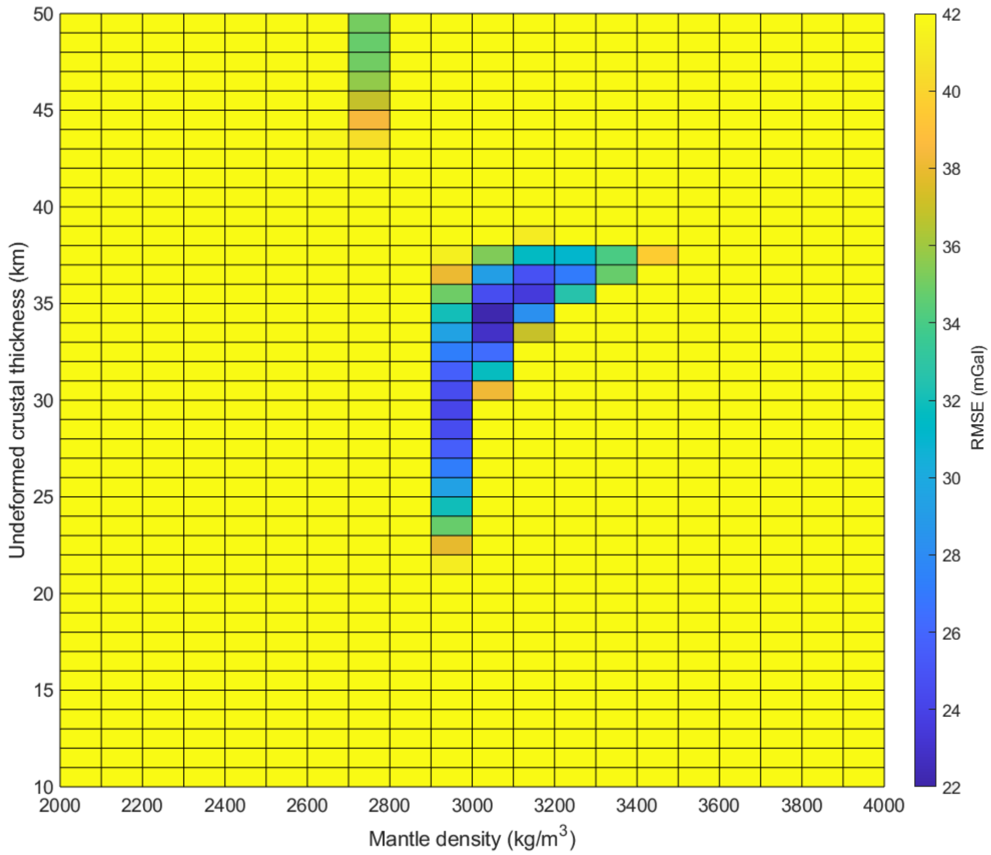

Figure S1. Root mean square error (RMSE) between the observed and predicted FAA to obtain best non-deformed crustal thickness and density variation between Mantle and Crust. Moho data constrained from (Torne et al., 2020) and FAA from WGM2012 (Bonvalot et al., 2012). The predicted model assumes constant crustal density of 2800 kg/m^3. RMSE of best fit is 22 mGal at $\Delta\rho = 500$ kg/m^3.

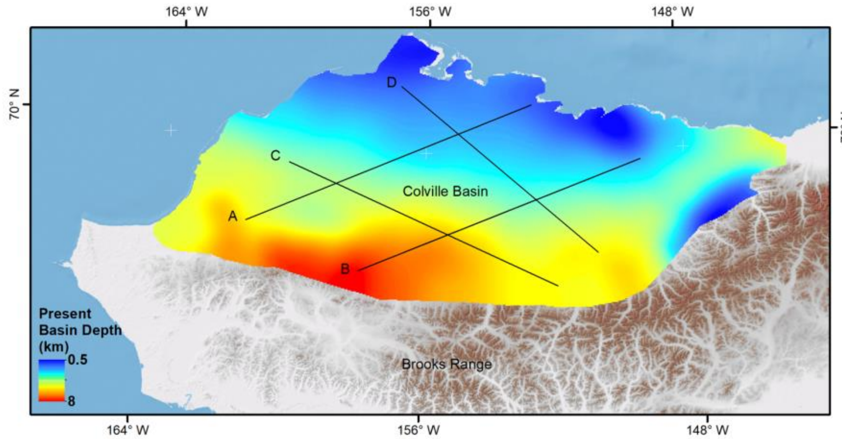

Figure S2. Location of sections for Figure S2 and S3.

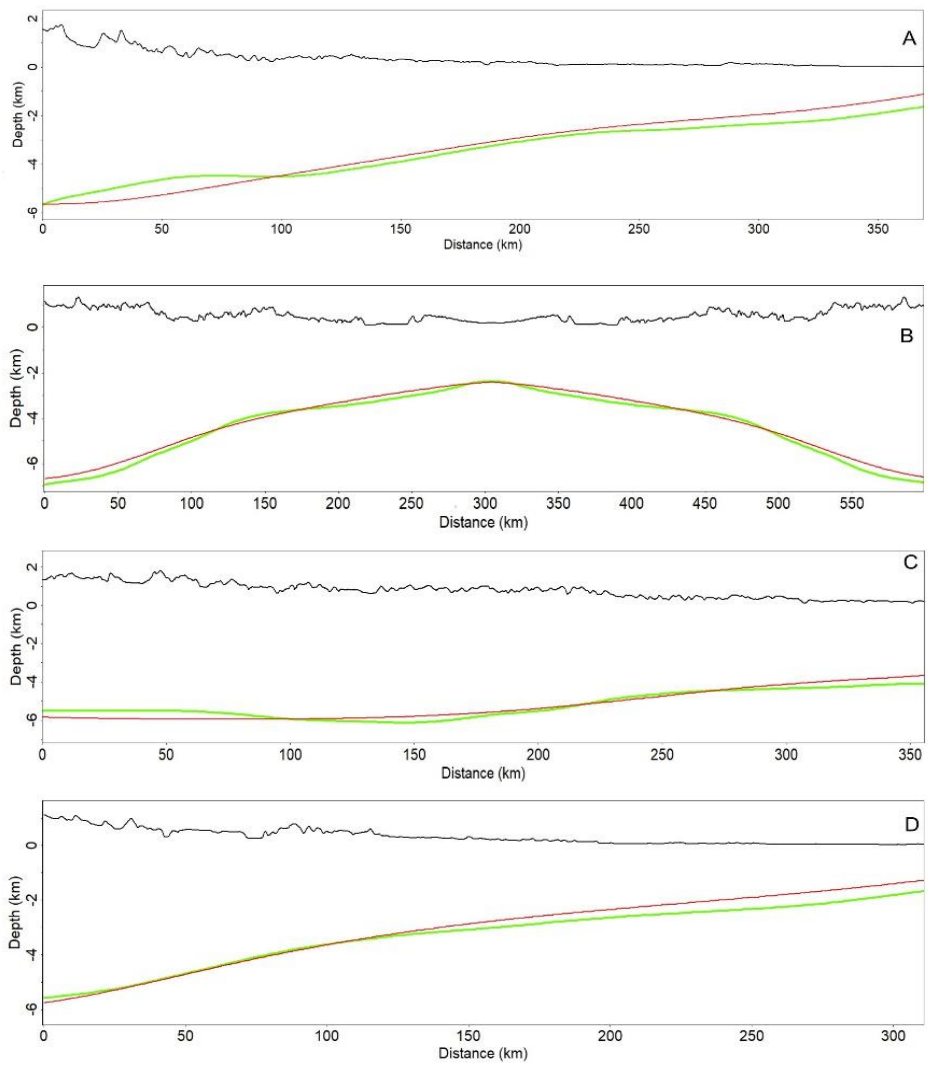

Figure S3. Best fit cross-sections (red curve) compared to observed data (green) in the Colville foredeep. Topography (black) is 3x exaggerated. Location of sections shown in Figure S1.

Figure S4. Calculated FAA from flexure model (red) and Moho data (yellow) compared with observed FAA (black) in the Colville foredeep. FAA from flexure model fits well to the observed anomalies and FAA calculated with Moho data shows some mismatch. Location of sections shown in Figure S1.

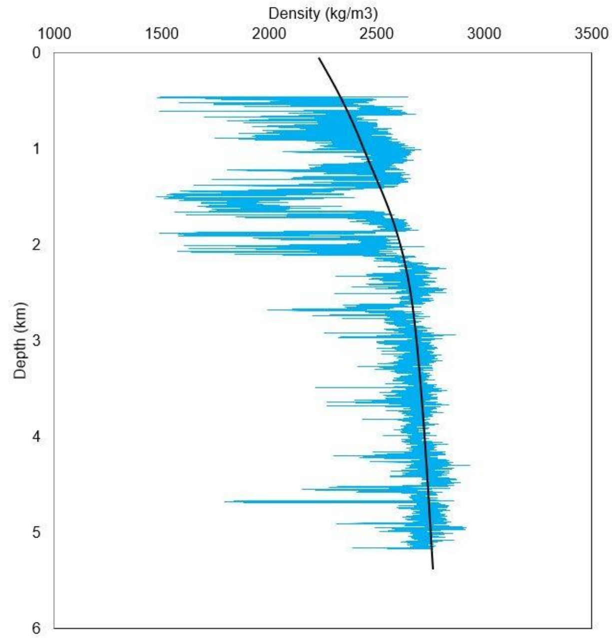

Figure S5. Vertical density variation with increasing depth in the Colville basin. The blue curve represents the measured density in the borehole. The black curve corresponds to a polynomial function that averages the depth distribution of density. The well is located at the southernmost edge of the Colville foredeep. See the green circle in (Figure 1) main text for the location of density log. Well data is available from USGS NPRA datasets at https://certmapper.cr.usgs.gov/data/apps/npra/.

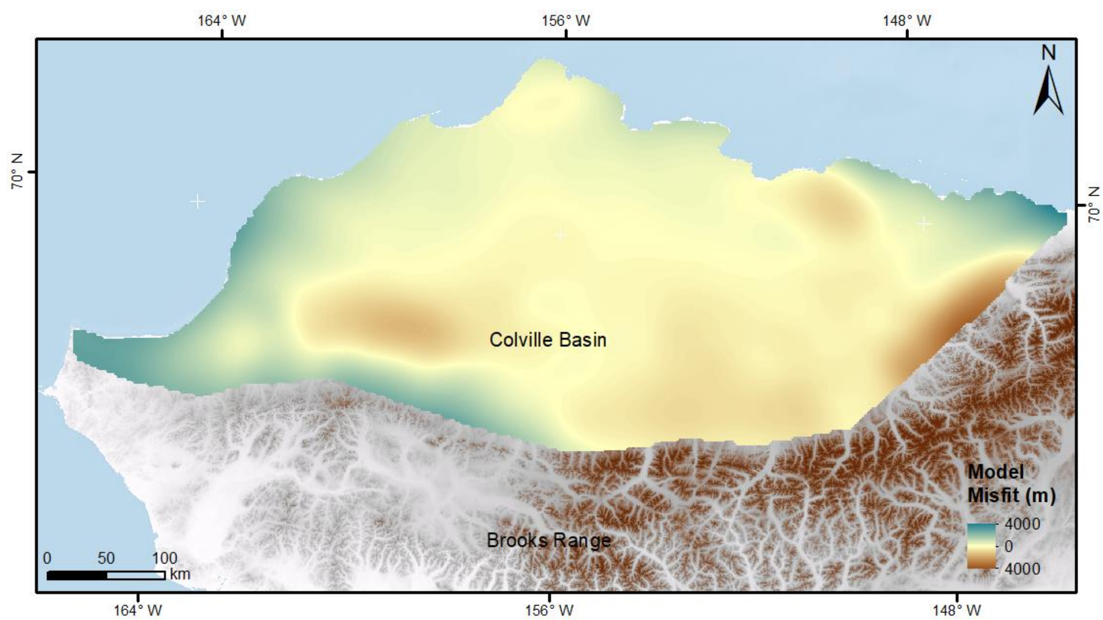

Figure S6. Misfit of flexure model shown with colormap. Yellow color characterizes the minimum misfit which covers significant part of the basin and blue and brown highlights regions of maximum misfit.